Brain, Behavior, and Immunity 117 (2024) 224–241

Contents lists available at ScienceDirect

Brain Behavior and Immunity

journal homepage: www.elsevier.com/locate/ybrbi

Full-length Article

Glia-derived adenosine in the ventral hippocampus drives pain-related anxiodepression in a mouse model resembling trigeminal neuralgia

Xue-Jing Lv [a], Su-Su Lv [a], Guo-Hong Wang [a], Yue Chang [a], Ya-Qi Cai [a], Hui-Zhu Liu [a], Guang-Zhou Xu [b,*], Wen-Dong Xu [a,c,*], Yu-Qiu Zhang [a,*]

[a] Department of Translational Neuroscience, Jing'an District Centre Hospital of Shanghai, State Key Laboratory of Medical Neurobiology and MOE Frontiers Center for Brain Science, Institutes of Brain Science, Fudan University, Shanghai 200032, China
[b] Department of Oral Surgery, Shanghai Ninth People's Hospital, Shanghai Jiao Tong University School of Medicine, Shanghai 200023, China
[c] Department of Hand Surgery, Huashan Hospital, Fudan University, Shanghai 200040, China

ARTICLE INFO

Keywords:
Adenosine
Anxiodepression
Astrocyte
Microglia
Trigeminal neuralgia
Ventral hippocampus

ABSTRACT

Glial activation and dysregulation of adenosine triphosphate (ATP)/adenosine are involved in the neuropathology of several neuropsychiatric illnesses. The ventral hippocampus (vHPC) has attracted considerable attention in relation to its role in emotional regulation. However, it is not yet clear how vHPC glia and their derived adenosine regulate the anxiodepressive-like consequences of chronic pain. Here, we report that chronic cheek pain elevates vHPC extracellular ATP/adenosine in a mouse model resembling trigeminal neuralgia (rTN), which mediates pain-related anxiodepression, through a mechanism that involves synergistic effects of astrocytes and microglia. We found that rTN resulted in robust activation of astrocytes and microglia in the CA1 area of the vHPC (vCA1). Genetic or pharmacological inhibition of astrocytes and connexin 43, a hemichannel mainly distributed in astrocytes, completely attenuated rTN-induced extracellular ATP/adenosine elevation and anxiodepressive-like behaviors. Moreover, inhibiting microglia and CD39, an enzyme primarily expressed in microglia that degrades ATP into adenosine, significantly suppressed the increase in extracellular adenosine and anxiodepressive-like behaviors. Blockade of the adenosine A2A receptor (A2AR) alleviated rTN-induced anxiodepressive-like behaviors. Furthermore, interleukin (IL)-17A, a pro-inflammatory cytokine probably released by activated microglia, markedly increased intracellular calcium in vCA1 astrocytes and triggered ATP/adenosine release. The astrocytic metabolic inhibitor fluorocitrate and the CD39 inhibitor ARL 67156, attenuated IL-17A-induced increases in extracellular ATP and adenosine, respectively. In addition, astrocytes, microglia, CD39, and A2AR inhibitors all reversed rTN-induced hyperexcitability of pyramidal neurons in the vCA1. Taken together, these findings suggest that activation of astrocytes and microglia in the vCA1 increases extracellular adenosine, which leads to pain-related anxiodepression via A2AR activation. Approaches targeting astrocytes, microglia, and adenosine signaling may serve as novel therapies for pain-related anxiety and depression.

1. Introduction

Mood disorders are frequently experienced by people suffering from chronic pain. Approximately one-third of individuals with chronic pain have numerous clinically relevant symptoms, such as irritability, anxiety and depression (Mills et al., 2019). These mood disorders are often overlooked and undertreated, leading to a further decline in the quality of life of patients. One advantage of preclinical studies is that animal models can mimic various aspects of chronic pain and anxiodepression, which is helpful for investigating and understanding the neurobiological substrates of anxiodepressive consequences of chronic pain-related anxiodepression. Our previous studies demonstrated that resembling trigeminal neuralgia mice developed allodynia and anxiodepressive-like behaviors in a time-dependent manner (Chen et al., 2023).

Mounting evidence indicates that glial elements are involved in the neuropathology of several neuropsychiatric illnesses including chronic pain and depression (Ji et al., 2016; Kimura et al., 2022; Klawonn et al., 2021; Yue et al., 2017). Both clinical and preclinical studies showed abnormal activation of microglia and astrocytes in several emotion-related brain areas, such as the prefrontal cortex and hippocampus, in

* Corresponding authors at: Institutes of Brain Science, Fudan University, #B5-005 Research Building 2B, 131 Dong An Road, Shanghai 200032, China.
E-mail addresses: xgzmy@163.com (G.-Z. Xu), wendongxu@fudan.edu.cn (W.-D. Xu), yuqiuzhang@fudan.edu.cn (Y.-Q. Zhang).

https://doi.org/10.1016/j.bbi.2024.01.012
Received 13 September 2023; Received in revised form 11 December 2023; Accepted 14 January 2024
Available online 18 January 2024

chronic pain patients (Loggia et al., 2015) and animal models of neuropathic pain (Hisaoka-Nakashima et al., 2019; Phelps and LeDoux, 2005), which might contribute to comorbid neuropathic pain comorbid with anxiodepression (Liu et al., 2021). Microglia and astrocytes synthesize and release various pro-inflammatory cytokines, such as interleukin (IL)-1β and tumor necrosis factor (TNF)-α, which drive the pathogenesis of depressive-like phenotypes (Fenn et al., 2014; Leng et al., 2018; Skaper et al., 2014). Inflammation prompts astrocytes to release large amounts of the gliotransmitter adenosine triphosphate (ATP), which transforms into adenosine monophosphate (AMP) catalyzed by CD39 and is then hydrolyzed to produce adenosine (Benatti et al., 2016; Zhao et al., 2022). Alteration of ATP/adenosine has been proposed to underlie depressive-like behaviors (Cao et al., 2013; Chen et al., 2023; Duman and Aghajanian, 2012). Epidemiological data indicate that consumption of caffeine, a non-selective adenosine receptor antagonist, can reduce the risk of depressive symptoms (Lucas et al., 2011). The action of adenosine in the brain mainly depends on activation of the adenosine-inhibiting A1 receptor (A1R) and the adenosine-stimulating A2A receptor (A2AR), which are widely distributed in limbic brain areas including the hippocampus (Camargo et al., 2023; Kaster et al., 2015; Machado et al., 2017). The hippocampus, especially the ventral hippocampus (vHPC), plays a critical role in the affective and behavioral changes seen after nerve injury (Fasick et al., 2015; Fiore and Austin, 2019; Ma et al., 2019). However, how astrocytes and microglia regulate ATP/adenosine and neuronal activity in the vHPC, which in turn mediates chronic pain-induced anxiodepressive-like consequences remains incompletely understood.

In this study, by combining genetic and pharmacological approaches, we investigated the role of astrocyte–microglia communication in neuropathic pain-induced anxiodepression. We demonstrate that persistent cheek pain activates microglia and astrocytes in the CA1 area of vHPC (vCA1), and upregulates extracellular adenosine derived from glia, thereby increasing the activity of vCA1 pyramidal neurons, that in turn leads to anxiodepressive-like symptoms. Our analyses also suggest that A2AR could be a new target for treatments of chronic pain-related anxiodepression.

2. Materials and methods

2.1. Animals

Adult male and female C57BL/6J mice (6–12 weeks) were purchased from Shanghai Experimental Animal Center of the Chinese Academy of Sciences. Both male and female CX3CR1-CreER-GFP (JAX#021160), ChR2-Flox (JAX#012567) and Arch-Flox (JAX#012735) mice were from the Jackson Laboratory. CX3CR1-GFP::ChR2 and CX3CR1-GFP::Arch mice were bred by CX3CR1-CreER-GFP and ChR2-Flox and Arch-Flox mice, respectively. The source of animals is detailed in Supplementary Table 1. All animals were housed (4 mice per cage, length × width × height, 33 × 21 × 15 cm, clear plastic cage) on a 12/12 h light–dark cycle within a colony room at 22 °C, ~60 % humidity, and ~100 lx illumination. Food and water were provided *ad libitum*. We randomly assigned the body weight and sex (transgenic animals) of mice to experimental and control groups, and an investigator blinded to mouse genotypes/treatments and group assignments tested them. All the animal experiments were approved by the Committee on the Use of Animal Experiments of Fudan University (Permit No. SYXK 2009–0082), and conducted by following the guidelines for pain research of the International Association for the Study of Pain.

2.2. Chronic constriction injury of the infraorbital nerve

The resembling trigeminal neuralgia mouse model was constructed by chronic constriction of the unilateral infraorbital nerve (CION) via an intraoral approach as described previously (Sheng et al., 2020). In brief, mice were anaesthetized with intraperitoneal (i.p.) injection of sodium pentobarbital (50 mg/kg) and the head was fixed, keeping the body supine and mouth wide open. A surgical incision was made at 0.1 cm proximal to the first molar along the left gingivobuccal margin, and the left infraorbital nerve was exposed. One ligature with 5–0 chromic gut catgut was tied loosely around the nerve. Sham-operated mice received only nerve exposure without ligation. All surgical procedures were performed aseptically.

2.3. Virus and stereotaxic injection

Mice were anesthetized with sodium pentobarbital (50 mg/kg, i.p.) and then fixed on a mouse stereotaxic apparatus (51725D, Stoelting, USA). The skull plane was adjusted to ensure that the bregma and lambda were at a horizontal level. A small craniotomy hole was made using a dental drill, and a heating pad was used to maintain the body temperature at 37 °C during anesthesia. A volume of 200–300 nL (depending on the expression strength and viral titer) virus was injected through a glass microelectrode attached to a microinjection pump (Hamilton, Nanoliter 2010 injector, World Precision Instruments Inc.) at a guaranteed rate 50 nL/min. The microelectrode injection needle was not withdrawn until 10 min after the end of infusion, allowing the virus to diffuse sufficiently. The stereotaxic coordinates for the vCA1 were + 3.2 mm anterioposterior (AP), 3.7 mm mediolateral (ML), and –3.5 mm dorsoventral (DV). Virus details are shown in Supplementary Table 1. AAV expression was permitted for at least 3 weeks before the experiments. The mice with off-target mCherry or EGFP localization were excluded from the analysis.

2.4. Intra-vCA1 drug infusions

Mice were anesthetized with sodium pentobarbital (50 mg/kg, i.p.) and placed in a stereotaxic apparatus. A stainless steel guide cannula (62004, RWD Life Science, Shenzhen, China) with stainless steel stylet plug (62104, RWD Life Science) was implanted above the injection site in the vCA1. The cannula was fixed by tissue glue and dental cement. Then, the animals were returned to their home cage and allowed to recover for 7 days. Microinjection was performed through an injector cannula (62204, RWD Life Science), which protruded 1.5 mm beyond the guide cannula to reach the site of vCA1. L-2-Aminoadipic acid (LAA, MilliporeSigma), Minocycline hydrochloride (MilliporeSigma), ARL 67156 (MilliporeSigma), Adenosine (Ado, MilliporeSigma), 8-phenyltheophylline (8-PT, MilliporeSigma), 3,7-Dimethyl-1-Propargylxanthine (DMPX, RBI), Gap27 and Gap27 scramble (Eurogentec) were dissolved in normal saline. A volume of 0.5 μL of vehicle or drug was injected at the rate of 0.1 μL/min. The injector cannula was held for 2 min before withdrawal to minimize drug spread along the injection track. Behavior tests were conducted after 30 min.

2.5. Optogenetic and chemogenetic experiments

CX3CR1-GFP::ChR2 and CX3CR1-GFP::Arch mice were used in the optogenetic manipulation of microglia experiments. We crossed CX3CR1-CreER mice, harbouring a tamoxifen-inducible Cre recombinase, with Ai35 mice carrying the floxed stop-Arch-EGFP gene in the ROSA26 locus, to generate the CX3CR1::Arch mice and also crossed CX3CR1-CreER line with floxed ChR2-tdTomato mice to generate the CX3CR1::ChR2 mice. Optical fibres (Ø200 μm Core, 3.5 mm length, Newdoon Technology Co., Ltd, Hangzhou, China) were implanted upon the mouse vCA1 (from bregma: AP − 3.2 mm; ML + 3.7 mm; and DV − 3.3 mm). Experiments were performed at 10 days after optical fibre implantation. Tamoxifen (50 mg/kg/day, i.p.) was injected into CX3CR1-GFP::Arch mice or CX3CR1-GFP::ChR2 mice for 3 days (Parkhurst et al., 2013). For the experiments of microglia inhibition, yellow light (580 nm, 5 mW, 1 h every day) was delivered into the vCA1 from Day 14 to Day 22 after CION. For the experiments of microglia activation, blue light (473 nm, 5 mW, 20 Hz, 30 min/day) was delivered into

the vCA1 for five continuous days.

To manipulate astrocytes, AAV-encoding halorhodopsin (eNpHR) or channelrodopsin-2 (ChR2) viruses driven by the astrocyte-specific promoter were injected into the vCA1. Four week after injection of optogenetic virus, optical fiber was implanted 0.2 mm above the virus injection site under anesthesia. Tissue glue and dental cement were applied to protect the hole of cortical surface and the skull window. Then the animals were allowed to recover for 7 days. Behavioral tests (EPM, TS, and *von* Frey) were performed with yellow light stimulation (580 nm, 5 mW,continuous) or blue light stimulation (473 nm, 5 mW, 20 Hz).

For chemogenetic inhibition, the designed CNO (5 mg/kg, i.p. C0832, Sigma-Aldrich, St Louis, MO, USA) was administered 30 min before behavioral tests.

2.6. Behavioral assessment

von Frey test The mouse was gently held by an experimenter wearing a regular leather work glove, and mechanical sensitivity was determined with a series of *von* Frey hairs (0.02, 0.04, 0.16, 0.4 and 0.6 g). The filaments were performed in an increasing order from the lowest force, and a brisk or active withdrawal of the head from the filament was considered a response. Each filament was tested five times at 15 s intervals. The withdrawal threshold was defined as the lowest force in grams that produced at least three withdrawal responses in five consecutive applications.

Elevated plus maze (EPM) The EPM device consisted of two closed arms (length × width: 30 cm × 6 cm), two open arms (length × width: 30 cm × 6 cm) and a central platform (length × width: 6 cm × 6 cm) elevated 50 cm above the floor. The two closed arms were enclosed with 20 cm-high walls crossing with two open arms. The room was maintained in a dim illumination (25 lx). Mice were gently placed in the central of the maze facing an open arm and were allowed to explore freely for 5 min. Movement of the animals in the maze was recorded with a digital camera over the maze. Open/closed arm entries and open arms time were analyzed with video tracking system (EthoVision XT v11.5, Noldus BV).

Open field (OF) test Open field test was performed in the open box (40 × 40 × 30 cm). The observation arena was divided into the angle zone (10 × 10 cm at the four corners) and the centre of the arena (20 × 20 cm). The surrounding was maintained in a dim illumination (25 lx) with no noise. Mice were gently placed into the centre of the arena and allowed to explore for 5 min. Video tracking software (EthoVision XT v11.5, Noldus BV) was used to record and analyse animal activities.

Tail suspension (TS) test The tail suspension box was made of plastic with the dimensions 30 cm × 30 cm × 30 cm (length × width × height). An aluminum suspension pole was positioned in the middle of the top of the box. The mice were suspended in the middle of the box with the tape at 0.1 cm proximal to the tail tip. The distance between the mouse's nose and the box floor was approximately 2 cm in the rest state. Mice activity was recorded with a digital camera for 6 min, and the immobility time in the last 4 min was counted.

2.7. Immunofluorescence staining and glia morphological analysis

Mice were sacrificed with overdoses of anesthetic and transcardially perfused with normal saline followed by pre-cold 4 % paraformaldehyde (PFA) in 0.1 M phosphate buffer (PB, pH 7.4). The brain was removed and postfixed in 4 % PFA for an additional 8–12 h at 4 °C. After dehydrated with gradient (10–30 %) sucrose in PB at 4 °C, coronary sections (30 μm) were cut on a cryostat microtome (Leica CM1950, Germany). The sections containing the ventral hippocampus were blocked with 10 % donkey serum with 0.3 % Triton X-100 for 2 h at room temperature (RT) and incubation overnight at 4 °C with corresponding primary antibodies: goat anti-ionized calcium-binding adapter molecule 1 (Iba1) (1:500, Abcam, Cambridge, UK), chicken anti-YFP/GFP (1:500, Aves, Tigard, OR, USA), rabbit anti-CD68 (1:500, Abcam), mouse anti-GFAP (1:2000, MilliporeSigma, St Louis, MO, USA), rabbit anti-CD39 (1:500, Abcam), rabbit anti-NeuN (1:2000, MilliporeSigma), goat anti-SOX9 (1:500, R&D Systems, MN, USA), rabbit anti-Adenosine A1 Receptor (1:500, Abcam), goat anti-A2AR (1:200, Frontier institute, Hokkaido, Japan), rabbit anti Connexin 43 (1:100, Invitrogen, CA, USA), rabbit polyclonal anti-IL-17 (1:50, Santa Cruz, Texas, USA) or mouse anti-IL-17RA/IL 17R (1:50, R&D Systems). The sections were then incubated with a mixture of Alexa Fluor 488- and 546-conjugated secondary antibodies (1:500, Invitrogen, Carlsbad, CA, USA; or Jackson ImmunoResearch, West Grove, PA, USA) for 2 h at 4 °C, or 4′,6-diamidino-2-phenylindole dihydrochloride (DAPI, 1:10,000, MilliporeSigma) for 5 min. The sources of the antibodies are detailed in Supplementary Table 1. The stained sections were observed and analyzed with a confocal microscope (Model FV1000, Olympus, Japan).

Hippocampal Iba-1 immunopositive microglia and GFAP immunopositive astrocyte were imaged with a confocal laser scanning microscope at 60 × magnification. The Neurolucida 360 software (MBF Bioscience, Williston, VT, USA) was applied for three-dimensional (3D) reconstruction of astrocytes and microglia within vCA1 area. Sholl analysis was performed to analyse the morphology of microglia and astrocytes by placing 3D concentric circles in 5 mm increments starting at 5 mm from the soma using the NeuroExplorer software.

2.8. Fluorescent in situ hybridization

Fluorescent in situ hybridization (FISH) was performed using the RNAscope system (Advanced Cell Diagnostics, ACD) according to the manufacturer's instructions. Sections were pretreated with hydrogen peroxide, target retrieval reagents and Protease III, and then treated for 2 h with IL-17RA mRNA probes (#566151, ACDBio), followed by AMP1, AMP2 and AMP3 successively for 15–30 min. The sections were further incubated in HRP-C3 for 15 min and Opal 690 (1:1500, PerkinElmer) for 30 min to fluorescently label the probe. Finally, HRP blocker was added for 15 min after fluorescent labeling of each channel. All hybridization and incubation steps were performed at 40 ℃ in the hybridization oven; moisture was maintained with the use of a wet box. GFAP immunohistochemical staining was continued after these procedures.

2.9. Western blotting

Mice were sacrificed with overdoses of anesthetic and the vHPC was rapidly isolated. The vHPC tissues were homogenized in lysis buffer (12.5 μL/mg) containing a mixture of protease inhibitors and phenylmethylsulfonyl fluoride (Roche Diagnostics, Indianapolis, USA). The protein concentration was determined by a BCA protein assay kit (Pierce, Rockford, Illinois, USA) according to its instruction provided by manufacturers. Protein samples (~30 μg) were loaded and separated on 10 % sodium dodecyl sulfate–polyacrylamide gel electrophoresis (SDS–PAGE, Bio-Rad, Hercules, CA, USA) and transferred to polyvinylidene difluoride membranes (PVDF, Millipore, Billerica, MA, USA). After blocked with 10 % non-fat milk at RT for 2 h, the membranes were incubated overnight at 4 °C with primary antibodies, followed by horseradish peroxidase (HRP)-conjugated secondary antibodies (1:10,000; Pierce, Rockford, Illinois, USA) for 2 h at 4 °C. GAPDH antibody was probed as a loading control. Signals were detected by enhanced chemiluminescence (ECL, ThermoFisher, 34095) and captured by ChemiDoc XRS System (Bio-Rad). We used the following primary antibodies: mouse anti GFAP (1:2000, #G6171, MilliporeSigma), goat anti Iba1 (1:500, #ab5076, Abcam) and rabbit anti CD39 (1:500, #ab227840, Abcam). All the Western blot analysis was performed three times and consistent results were obtained. ImageJ was then used to measure the integrated optic density of the specific bands.

2.10. RNA isolation and real-time polymerase chain reaction analysis

Mouse vHPC tissue was homogenized in TRIzol reagent (Invitrogen). Total RNA was extracted and reverse transcribed in accordance with the manufacturer's instructions (TAKARA, Japan). All polymerase chain reactions were performed using the TB Green™ Premix Ex Taq™ II kit (TAKARA) on a real-time polymerase chain reaction (PCR) system (QuantStudio™ 3, Thermo). Each sample was analyzed at least in triplicate; data were acquired and visualized using QuantStudio software (Applied Biosystems). β-actin was used as an internal reference. Details of the primer sequenches are shown in Supplementary Table 2. The relative expression level (with β-actin as the reference gene) were calculated from Ct values of the target and β-actin using the following formula: relative expression $= 2-(Ct_{target} - Ct_{\beta\text{-actin}})$.

2.11. Microdialysis and adenosine/ATP assay in the vCA1

The microdialysis probe (MD-2211, BASi, West Lafayette, IN, USA) was inserted into the bilateral vCA1 area via the guide cannula (MD-2255, BASi) to 1 mm beyond the tip of the guide cannula under sodium pentobarbital anaesthesia. The dialysis probe was connected to a microinfusing pump (BASi, Microdialysis Syringe 1.0 mL). The probe was perfused with artificial cerebrospinal fluid (ACSF) at a flow rate of 1 μL/min. After dialysate levels stabilized (about 1 h), sample was collected. To prevent degradation of Adenosine and ATP, EHNA hydrochloride (MilliporeSigma) and ecto-ATPase (ARL 67156, Sigma-Aldrich) were applied as the perfusate, respectively. At the end of the experiments, the mice were sacrificed with overdoses of anesthetic, and brains were sectioned to verify the position of the cannula. The Adenosine concentration was assessed by an Adenosine Assay Kit (BioVision, K327-100). According to the manufacturer's protocols, samples (50 μL) added to the wells with 50 ul reaction mix. And measure fluorescence immediately on a microplate reader at Ex/Em = 535/587 nm. The ATP concentration was assessed by an ENLITEN ATP Assay System with a bioluminescence detection kit (Promega, Madison, WI, USA). According to the manufacturer's protocols, samples (90 μL) were neutralized to pH 7.4 with 10 μL of 4 M Tris and the luciferase reagent was added 1 s before a 5 s measurement in a luminometer. Light photons were measured by the luminometer and compared with the standard curve to calculate ATP concentration.

2.12. ELISA assay

BV2 microglial cells were cultured in Dulbecco's modified Eagle's medium (DMEM) (Gibco) with 10 % FBS (Gibco) and 1 % penicillin/streptomycin (Gibco) at a humidified incubator at 37 °C with 5 % CO_2. The cells were treated with LPS (1 μg/mL, #L2880, Sigma) or minocycline (50 μg/mL) plus LPS for 24 h. The culture medium was collected. ELISA was conducted according to the manufacturer's instructions to assay IL-17A content by Mouse IL-17A High Sensitivity ELISA Kit (#EK217HS, Multi sciences (LianKe) Biotech, Hangzhou, China). The absorbance of the samples was measured at 450 nm using a microplate reader (Infinite M200, TECAIV).

2.13. Primary culture of vHPC astrocytes

Primary cultures of vHPC astrocytes were obtained from newborn mice. The vHPC tissues were removed under a microscope and immediately transferred onto Dulbecco's modified Eagle's medium (DMEM)/F12 (#11330032, Gibco) on ice. The minced tissue was treated with DMEM/F12 solution containing 0.25 % trypsin (#25200—072, Gibco) at 37 °C for 15 min. Digestion was terminated by adding an equal volume of medium containing fetal bovine serum (FBS), and cells were filtered through a 70-μm filter. Individual cells were centrifuged at 1,000 rpm for 5 min at room temperature, and medium containing 10 % FBS was added to diluted to 5×10^5 cells/mL. The diluted cell suspension was transferred to T25 cell culture flasks that had been pretreated with poly-D-lysine (0.1 mg/mL, #P0899, Sigma) for 2 h at 37 ℃ (approximately 5 mL of cell suspension per flask). The cells were incubated in a constant-temperature CO_2 incubator (5 % CO_2 , 37℃), and the medium was changed at full volume after 1 day and then at half volume every 3 days. After 3 weeks of culture, astrocytes were purified and transferred to six-well plates for further culture. Experiments were carried out according to cell growth after 2 weeks of culture. The medium contained 10 % FBS (#10099141, Gibco) and 1 % penicillin/streptomycin (#15140122, Gibco). Astrocytes cells were pretreated with IL-17A (100 ng/mL, #7956-ML-025/CF, R&D Systems) or IL-17RA antibody (10 μg/mL, #MAB4481, R&D Systems) plus IL-17A. After the final incubation, the astrocytes were collected for western blot.

2.14. Slice preparation and whole-cell patch clamp recordings

Mice were deeply anesthetized and transcardially perfused with ice-cold cutting solution (20 mL) containing (in mM) 92 NMDG, 2.5 KCl, 1.2 NaH_2PO_4, 20 HEPES, 30 $NaHCO_3$, 25 glucose, 5 Na-ascorbate, 3 Na-pyruvate, 2 thiourea, 10 $MgSO_4$, and 0.5 $CaCl_2$ (pH 7.3, 300–310 mOsm/L). The brains were quickly removed and submerged in pre-oxygenated (95 % O_2, 5 % CO_2, v/v) cold cutting solution. Slices (300 μm) containing the vHPC were cut using a vibrating microtome (VT1200S, Leica, Germany) and transferred to an oxygenated chamber filled with recording artificial cerebrospinal fluid (recording ACSF) containing (in mM) 119 NaCl, 2.3 KCl, 1 NaH_2PO_4, 26.2 $NaHCO_3$, 12 glucose, 1.3 $MgSO_4$, and 2.5 $CaCl_2$ (pH 7.3 when carbogenated with 95 % O_2 and 5 % CO_2, 300–310 mOsm/L) for 30 min at 32 ℃. The incubated brain slices were transferred to the recording chamber, and continuously perfused with circulated well-oxygenated ACSF at a rate of 2–3 mL/min at RT. The charge-coupled device (CCD) imaging system was used to find the vCA1 areas using the IR-DIC mode with a low-power lens (×10) and then switched to high-power lens (×60) in an Olympus BX51WI upright microscope to find the pyramid neurons.

Whole-cell patch clamp recordings were performed with Axon 700B amplifier with a Digidata 1550B digitizer (Axon Instruments). Patch pipettes (5–10 MΩ) were made of borosilicate glass on a horizontal micropipette puller (P-1000, Sutter Instruments, Novato, CA, USA). The signals were low-pass filtered at 2 kHz, digitized at 10 kHz, and analyzed with Clampfit 10.6 software (Molecular Devices). The current-evoked action potentials (APs) were recorded in current-clamp mode, and injected current steps from −50 pA to 200 pA steps. The pipette solution containing (in mM) 125 K-gluconate, 15 KCl, 0.5 EGTA, 10 HEPES, 10 phosphocreatine, 2 Mg-ATP, and 0.5 Na-GTP (pH 7.3, 300–310 mOsm/L).

2.15. Imaging of calcium, ATP, and adenosine in vHPC slices

GCaMP6, ATP1.0, and Ado_B10 viruses were injected into the vCA1 as described above. Three weeks later, mice were sacrificed, and the slices were prepared in the same manner as for whole-cell patch clamp recording. GCaMP6-, ATP1.0-, or Ado_B10-positive cells in the vCA1 area were identified and imaged using a charge-coupled device (CCD, ORCA-Flash 4.0, Hamamatsu, Japan) and a microscope (Olympus, BX51WI) using a 60 × objective. Images were acquired at a rate of 1 frames/s (1024 × 1024 pixels) using HCImage Live software (Hamamatsu Photonics, Shizuoka, Japan). Biosensors of GCaMP6, ATP1.0, and Ado_B10 were excited at 480 nm. Optical stimulation was provided by a light-emitting diode (LED, X-cite 110, USA) connected to a programmable pulse stimulator (Master-9, AMPI, Israel). Emitted fluorescence was collected using a 535-/540- nm filter for GCaMP6, ATP1.0, and Ado_B10. To record glial calcium signals, tetrodotoxin (TTX, 0.5 μM) and a cocktail of neurotransmitter receptor antagonists were added to the perfusate to exclude any influence of neurons. The cocktail antagonists includes CNQX (AMPA/Kainate receptor antagonist, 20 μM), APv (NMDA receptor antagonist, 50 μM), MPEP (mGluR5 antagonist, 50

μM), LY 367385 (mGluR1a antagonist, 100 μM), CGP 55845 ($GABA_B$ receptor antagonist, 10 μM), Picrotoxin ($GABA_A$ receptor antagonist, 50 μM), and atropine (mAchR antagonist, 50 μM). IL-17A (200 ng/mL, 5 s), ATP (100 μM, 5 s) or vehicle (ACSF) was puff-applied using a pulled glass capillary (P-1000 Micropipette Puller; Sutter Instrument, Novato, CA, USA). DL-fluorocitric acid barium salt (FC, 10 μM, MilliporeSigma), ARL 67156 (ARL, 100 μM), or Gap27/scramble (100 μM) was added to the perfusate. Time-lapse fluorescence images of the brain slices were then imported into Fiji software (NIH, Bethesda, MD, USA) as TIFF files for analysis of fluorescence intensity. The data were analyzed using the CalmAn package. Time traces of fluorescence intensity were extracted from the region of interest (ROI) and converted into ΔF/F values (background-corrected increase in fluorescence divided by the baseline fluorescence), and area under the curve (AUC) values were calculated for individual cells. The heat map was plotted using MATLAB (MathWorks, Natick, MA, USA).

2.16. Fiber photometry

Fiber photometry was performed as reported previously (Tang et al., 2022). Adeno-associated virus (AAV)-hSyn-Ado_B10 virus was injected into the vCA1 as described above. Two weeks later, an optical fiber (Ø200 μm Core, 3.5 mm length) was implanted 0.2 mm above the virus injection site. The mice were allowed to recover for at least 7 days. Ado_B10 fluorescence was recorded using a fiber photometry system (FPS-MC-LED, Thinker Tech).

To assess the vCA1 extracellular adenosine signal arising in response to TS exposure, the mice were placed in a box and movement (struggling vs. immobility) was recorded simultaneously with Ado_B10 (adenosine sensor) fluorescence signal. Adenosine-dependent fluorescent signals were recorded in Ado_B10-expressing vCA1 neurons using a 470-nm laser. The laser power at the tip of the optical fiber was adjusted to 30 μW to reduce laser bleaching. The moment at which each mouse transitioned from struggling to immobility was defined as event onset. The average fluorescent signal 2 s before event onset was taken as the baseline. The ΔF/F and AUC values of the Ado_B10 fluorescence signal corresponding to events were analyzed. Heat maps and averaged fluorescence signals were plotted using MATLAB.

2.17. Statistical analysis

The data are presented as mean ± standard error of the mean (SEM). Data from different groups were verified for normality and homogeneity of variance using Shapiro-Wilk and Brown-Forsythe tests before analysis, where no data were transformed. No data were excluded from statistical analysis due to outlier status. Comparisons between two groups were performed using Student's *t* test, or Mann-Whitney *U* test (nonparametric data). Comparisons among three or more groups were performed using one-way or two-way ANOVA followed by *post-hoc* Sidak test or Kruskal–Wallis H test followed by *post-hoc* Dunn's test (nonparametric data). All analyses were two-tailed and a P-value less than 0.05 ($p < 0.05$) was considered statistically significant. Statistical analyses were performed using Graphpad Prism 8.0 software (GraphPad Software, San Diego, CA, USA).

3. Results

3.1. Increased extracellular adenosine in the vCA1 contributes to CION-induced anxiodepression

A rTN mouse model was established by chronic constriction of the infraorbital nerve (CION) to mimic clinical trigeminal neuropathic pain. After CION, mechanical allodynia was observed in the ipsilateral vibrissa pad on the day 2 and persisted for at least 21 days (Supplementary Fig. 1A and B). Tests conducted from day 14 after CION revealed anxiodepressive-like behaviors in line with our previous study (Chen et al., 2023). CION mice spent less time in open arms, and had fewer open arm entries, in the elevated plus maze (EPM) test. Moreover, they showed a decrease in the number of vertical activity and spent less time in the central area in the open field (OF) test, and were immobile for longer in the TS test (Supplementary Fig. 1C–F). We also observed similar behavioral phenotype in female mice after CION (Supplementary Fig. 1G-K). There was no difference between the CION and sham groups in total travel distance in the OF test, indicating that the CION-induced anxiodepressive-like behavioral phenotypes were not due to motor impairment.

Dysregulation of extracellular ATP/adenosine and the purinoceptors P1 and P2 is involved in the pathophysiology of depression (Bartoli et al., 2020; Cao et al., 2013; Zou et al., 2023). Our recent study showed that hippocampal ATP-P2X7 receptor signaling was involved in chronic pain-induced anxiodepressive-like symptoms (Chen et al., 2023). We further investigated the role of the ATP metabolite adenosine, and the P1 receptors A1R and A2AR in CION-induced anxiodepression. To determine whether neuropathic pain alters extracellular adenosine levels in the vCA1, we measured the extracellular adenosine concentration in the dialysate in the vCA1 on day 14 after CION. Compared with sham mice, the extracellular adenosine level was significantly increased in the vCA1 in CION mice (Fig. 1A). We also used optical fiber photometry to measure extracellular adenosine by expressing genetically encoded fluorescent GPCR activation-based (GRAB) sensors for adenosine (Ado_B10) in vCA1 neurons (Peng et al., 2020). Increased adenosine sensor fluorescence intensity was observed when mice with rTN transitioned from struggling to immobility (despair) in the TS test (Fig. 1B, C). These data suggest that the extracellular adenosine level in the vCA1 was increased on day 14 after CION.

Extracellular adenosine mainly binds to the high-affinity A1R and A2AR both of which were detected in the vCA1 and mainly colocalized with the neuronal marker Nissl (Supplementary Fig. 2A, B). Real-time polymerase chain reaction (PCR) analysis showed that either *Adora1* or *Adora2a* mRNA significantly increased on day 14 after CION (Supplementary Fig. 2C, D). To determine whether A1R and A2AR play a role in CION-induced anxiodepressive-like behaviors, we administered the selective A1R antagonist 8-phenyltheophylline (8-PT, 10 nmoL), and the A2AR antagonist 3,7-dimethyl-1-propargylxanthine (DMPX, 15 nmoL) into the vCA1. DMPX, but not 8-PT, significantly ameliorated CION-induced anxiodepressive-like behaviors in the EPM and TS tests (Fig. 1D-H). Neither DMPX nor 8-PT affected CION-induced mechanical allodynia (Fig. 1I). Furthermore, we selectively knocked down A2AR in excitatory neurons vCA1 through adeno-associated virus AAV-expressing A2AR-short-hairpin RNA (shRNA, Fig. 1J). Knockdown efficiency was confirmed by immunofluorescence staining and quantitative PCR. (Fig. 1K, L). Knockdown of A2AR in excitatory CaMK2A-positive pyramidal neurons in the vCA1 significantly blocked anxiodepressive-like behaviors in CION mice without affecting mechanical allodynia (Fig. 1M-P). In particular, attenuation of anxiodepressive-like behaviors and the knockdown efficiency of A2AR had a linear relationship (Fig. 1P). We also examined the effects of knocking down A2AR on anxiety and depression severity in normal mice. No statistical differences were detected between the A2AR-shRNA and control groups (Supplementary Fig. 2E–I). Next, we determined whether adenosine elicits anxiodepressive-like behaviors directly. Microinjection of adenosine (10 nmoL) into the vCA1 produced typical anxiodepressive-like behaviors, including fewer entries into the open arms of the EPM and more time spent immobile time in the TS test (Supplementary Fig. 2J–M). The effects of adenosine were attenuated by the A2AR antagonist DMPX but not by the A1R antagonist 8-PT. Taken together, the data suggest that adenosine in the vCA1 may function mainly through activation of the A2AR.

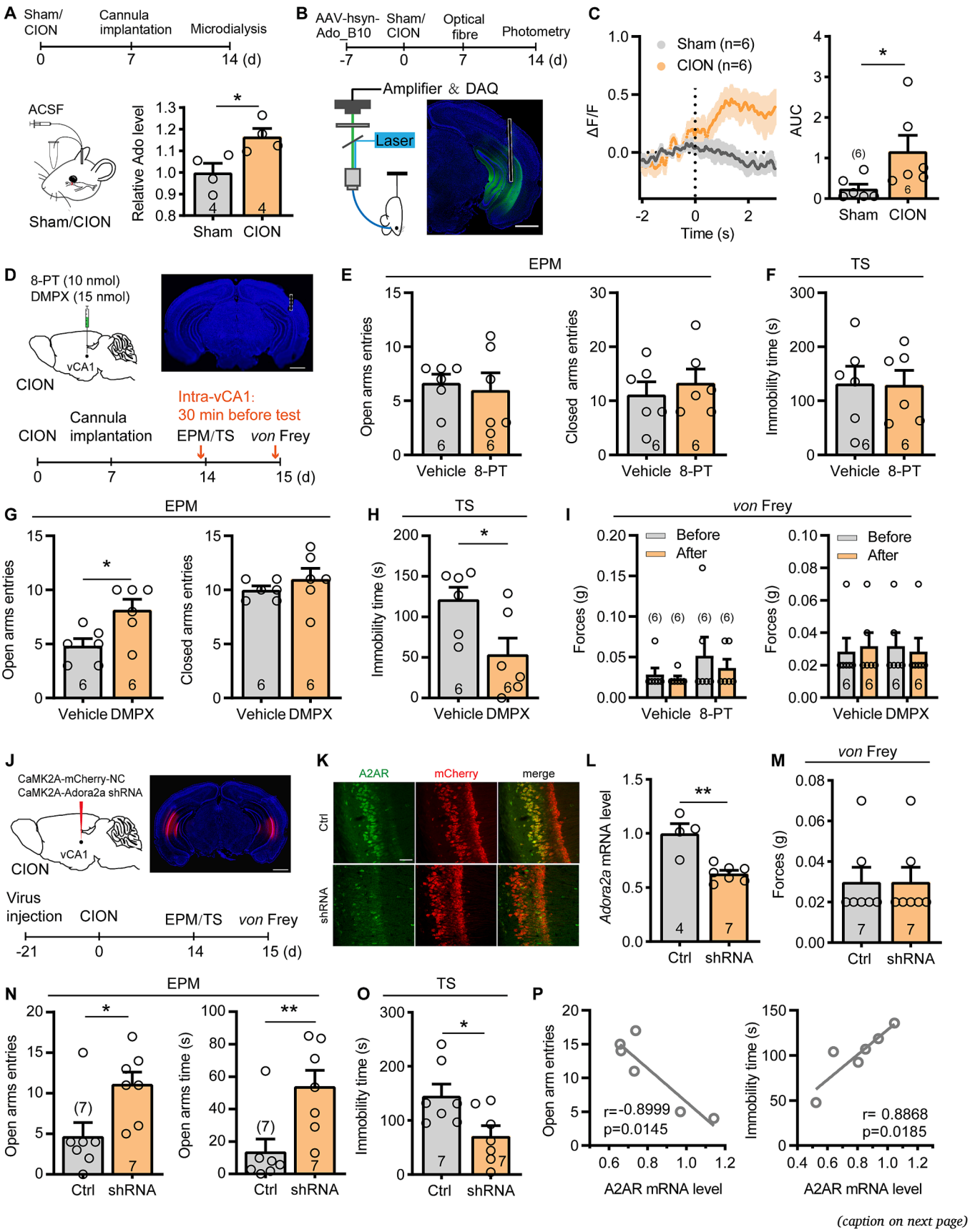

(caption on next page)

Fig. 1. Adenosine A2A receptors (A2ARs) in the CA1 area of the ventral hippocampus (vCA1) contribute to CION-induced anxiodepressive-like behaviors. (A) Microdialysis showed a significant increase in the extracellular adenosine level in the vCA1 on day 14 after constriction of the infraorbital nerve (CION). (B) Schematic and photomicrograph of a coronal section showing the protocol for in vivo optical fiber photometry recording and the sites of optical fiber implantation and Ado_B10 (an adenosine sensor) expression in the ventral hippocampus (vHPC). Scale bar: 1 mm. (C) Average change in Ado_B10 fluorescence (left) and area under the curve (AUC; right) values indicated an increase in extracellular adenosine as the mouse transitioned from struggling to immobility during the tail suspension (TS) test on day 14 after CION. (D) Sagittal schematic and photomicrograph of a coronal section showing the site of drug injection into the vCA1 and the cannula position, and the protocol for experiments E–I. Scale bar: 1 mm. (E and F) Intra-vCA1 injection of the adenosine A1 receptor (A1R) antagonist 8-phenyltheophylline (8-PT) did not affect CION-induced anxiodepressive-like behaviors in the elevated plus maze (EPM; E) or TS (F) test. (G and H) Intra-vCA1 injection of the A2AR antagonist 3,7-dimethyl-1-propargylxanthine (DMPX) significantly alleviated CION-induced anxiodepressive-like behaviors. (I) Neither 8-PT nor DMPX affected CION-induced mechanical allodynia. (J) Sagittal schematic and photomicrograph of a coronal section showing adeno-associated virus (AAV)-short hairpin (shRNA)-mCherry injection into the vCA1 and the protocol for experiments M−O. Scale bar: 1 mm. (K and L) Knockdown of A2AR was confirmed by immunohistochemistry (K) and real-time polymerase chain reaction (PCR; L). Scale bar: 50 μm. (M−O) Knockdown of A2AR in CaMK2A-positive neurons of the vCA1 prevented the development of anxiodepressive-like behaviors in CION mice, but had no effect on mechanical allodynia. (P) The anti-anxiodepressive-like effects had a linear relationship with the knockdown efficiency of A2AR. Data are expressed as means ± SEM. *p < 0.05, **p < 0.01, two-tailed Student's *t*-test. Sample sizes are indicated in bars and brackets.

3.2. Activated astrocytes are required for CION-induced upregulation of extracellular adenosine

Accumulating evidence shows that ATP and its enzymatic degradation product, adenosine, are mainly produced in astrocytes (Boison et al., 2010; Liu et al., 2019). Activated astrocytes release excessive ATP, a gliotransmitter, in various pathological conditions (Hamilton and Attwell, 2010; Zhao et al., 2022). Thus, we first examined whether astrocytes in the vCA1 are activated by CION. Western blot analysis showed robust elevation of glial fibrillary acidic protein (GFAP) in the vHPC on days 14 and 21, but not on day 5, after CION (Fig. 2A), which may be associated with the development of anxiodepressive-like behaviors according to our previous study (Chen et al., 2023). CION-induced activation of astrocytes was further confirmed by GFAP, S100β (another astrocytic marker), and SRY (sex determining region Y)-box 9 (SOX9, an astrocyte-specific nucleus marker) immunohistochemistry and *gfap* mRNA level by real-time PCR (Fig. 2B; Supplementary Fig. 3A–D). Morphologically, activated astrocytes exhibited enlarged soma and prolongated or more abundant processes (Fig. 2C-F).

Astrocytes secrete ATP via several pathways, most notably through connexin 43 (Cx43) hemichannel opening (Hamilton and Attwell, 2010; Kang et al., 2008; Torres et al., 2012). We therefore examined the effects of Cx43 blockade on the extracellular ATP/adenosine level in the vCA1. Corresponding to the activation of astrocytes, Cx43 immunoreactivity (IR) in the vCA1 was also significantly increased on day 14 after CION, and Cx43 was colocalized with GFAP-positive cells (Fig. 2G). Perfusion of the Cx43 mimetic peptide, Gap27 (100 μM), via a microdialysis probe completely blocked CION-induced increases in ATP and adenosine levels (Fig. 2H-J). Furthermore, the effect of silencing astrocytes on the extracellular ATP level in the vCA1 was examined. We injected a Gi-coupled inhibitory designer receptor exclusively activated by designer drugs (DREADD), and encoding AAV (driven by the GfaBC1D promoter), into the vCA1. GfaABC1D-mCherry signals were colocalized with GFAP-IR almost without exception (Fig. 2K and L). Chemogenetic inhibition of vCA1 astrocytes significantly attenuated CION-induced increases in ATP and adenosine levels in extracellular dialysate (Fig. 2M and N). To verify the inhibitory effects of Gi-coupled DREADD in astrocytes, we performed a prolonged calcium imaging in vHPC slices. Consistent with previous report by Kol et al. (Kol et al., 2020), Puff application of clozapine N-oxide (CNO, 3 μM) triggered a decrease in baseline intracellular Ca^{2+} levels in vCA1 astrocytes expressing both hM4Di-mCherry and GCaMP6 (Fig. 2K; Supplemental Fig. 4). These data indicate that activated astrocytes are the major source of ATP/adenosine in the vCA1 area of CION mice.

3.3. Activated microglia contribute to the increase of extracellular adenosine seen in CION mice through CD39

Extracellular ATP degradation via ectonucleotidase has been identified as a major source of adenosine (Boison et al., 2010; Zhao et al., 2022). Extracellular ectonucleotidase, also known as CD39, is a rate-limiting enzyme for ATP hydrolysis (Moesta et al., 2020). Considering that CD39 is primarily expressed by microglia (Badimon et al., 2020; Lanser et al., 2017), we next evaluated the activation of microglia in the vCA1 after CION. Consistent with the increased GFAP expression and anxiodepressive-like behaviors, significant upregulation of ionized calcium-binding adaptor molecule (Iba)-1 was also seen in the vHPC on day 14 after CION (Fig. 3A). CION-induced activation of microglia was further confirmed by Iba-1 and CD68 (a microglial activation marker) immunohistochemistry or real-time PCR (Fig. 3B, Supplementary Fig. 5A–D). Morphologically, activated microglia exhibited large cell bodies and short or thick processes in the vCA1 (Fig. 3C-F). Furthermore, the increase in CD39 induced by CION in the vCA1 was also detected on day 14 after CION (Fig. 3G and H). Double immunostaining revealed that CD39-IR was exclusively expressed in Iba-1-positive cells (Fig. 3I, Supplementary Fig. 5E). Perfusion with the CD39 inhibitor, ARL 67156 (100 μM) robustly suppressed extracellular adenosine in rTN mice (Fig. 3J). Similarly, the microglial inhibitor minocycline (Mino) effectively inhibited CION-induced upregulation of extracellular adenosine (Fig. 3J) and CD39-IR in the vCA1 (Fig. 3K). These results indicate that microglial CD39 is necessary for CION-induced upregulation of extracellular adenosine in the vCA1.

3.4. Activated microglia promote ATP release from astrocytes in the vCA1 area via IL-17A

Activated microglia synthesize and release a variety of pro-inflammatory cytokines. We detected elevated mRNA levels of TNFα, IL-1β, and IL-17A in the vHPC of rTN mice using real-time PCR (Supplementary Fig. 6A). Immunohistochemical data showed an increase in IL-17A-IR in the vCA1 of rTN mice, colocalized primarily with microglia (Fig. 4A and B). Lipopolysaccharide (LPS, 1 μg/mL)-stimulated BV2 microglial cells showed significantly higher *il-17a* mRNA levels (Fig. 4C) and increased IL-17A release in cultured medium (Fig. 4D). Minocycline (50 μg/mL) suppressed LPS-induced mRNA and protein expression of IL-17A after a 24-h treatment period (Fig. 4C, D). IL-17A signals through its receptor, IL-17RA, which was detected on astrocytes and neurons (Supplementary Fig. 6B and C). In primary cultured vHPC astrocytes, IL-17A (100 ng/mg) treatment robustly increased GFAP protein expression, although this was partially blocked by IL-17RA-neutralizing antibody (Supplementary Fig. 6D). Next, we used calcium imaging to assess IL-17A-induced changes in Ca^{2+} signaling on vCA1 astrocytes by injecting of AAV-encoding GCaMP6 virus driven by the GfaABC1D promoter (Fig. 4E). After ex vivo sectioning, puff application of IL-17A (200 ng/mL) evoked increased Ca^{2+} signaling in vCA1 astrocytes expressing the Ca^{2+} indicator GCaMP6 (Fig. 4F-H). During the Ca^{2+} signal recording, a cocktail of neurotransmitter receptor antagonists (CNQX, APV, MPEP, LY 367387, picrotoxin, CGP 55854, atropine) and TTX were added to the perfusate to prevent any effect of neuronal activity on astrocytic Ca^{2+} activity. A transient increase in the cytosolic Ca^{2+} concentration in astrocytes can trigger the release of gliotransmitters, including ATP (Araque et al., 2014; Hamilton and Attwell,

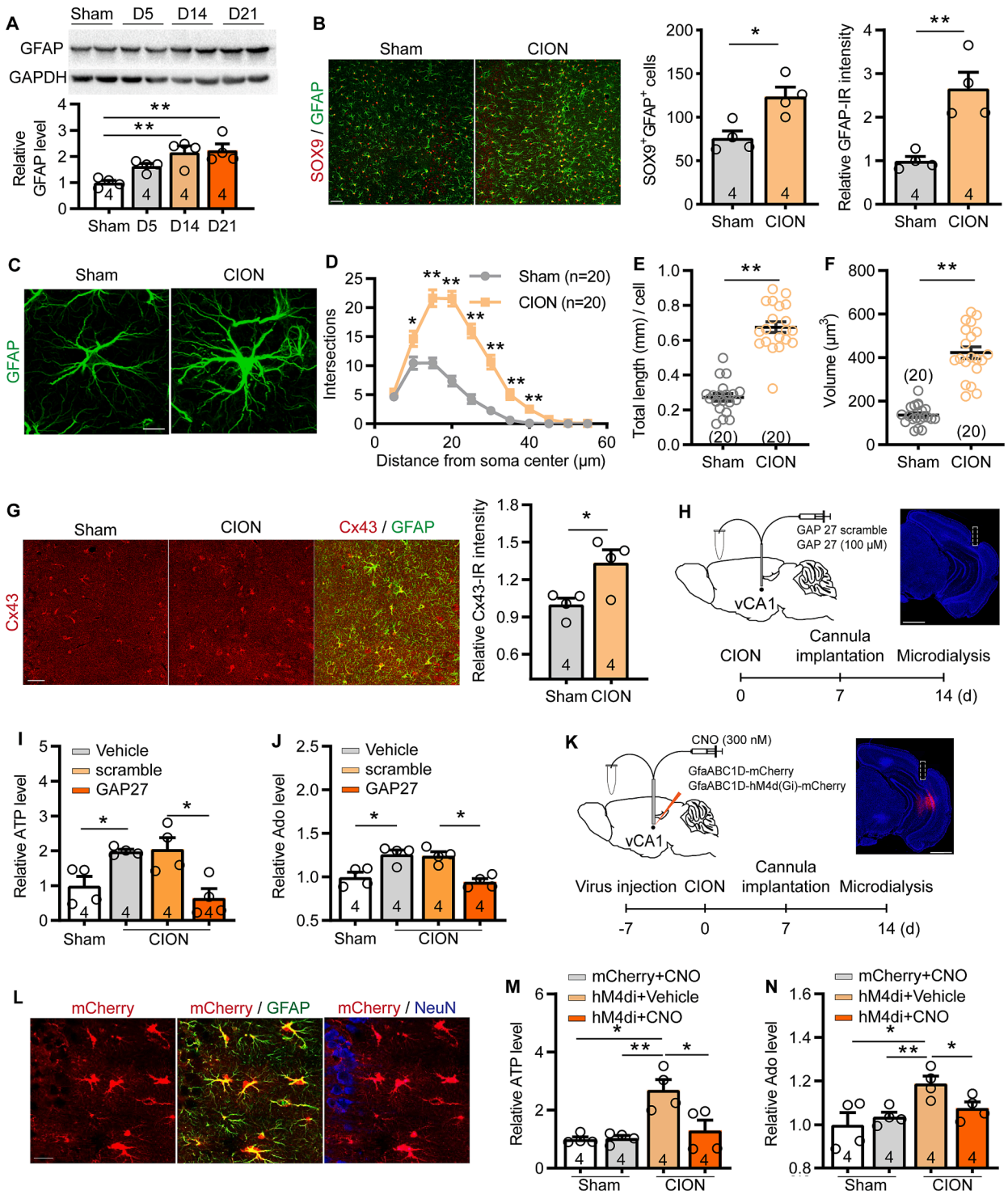

Fig. 2. Activated astrocytes and connexin 43 (Cx43) are involved in TN-induced increases in extracellular adenosine triphosphate (ATP)/adenosine. (A) Western blot analysis revealed significant upregulation of the astrocytic marker glial fibrillary acidic protein (GFAP) on days 14 and 21, but not day 5, after CION in the vHPC. (B) Immunofluorescence labeling showed astrocytic activation, as indicated by increases in GFAP immunofluorescence and the number of SOX9/GFAP double-positive cells in the vCA1. Scale bar: 50 μm. (C–F) Sholl analysis revealed prolongated or more abundant processes, and enlarged somas, in vCA1 astrocytes on day 14 after CION. Scale bar: 5 μm. (G) Immunofluorescence staining of Cx43 revealed increased Cx43 immunoreactivity (IR) in the vCA1 on day 14 after CION and colocalization with GFAP-IR. Scale bar: 30 μm. (H) Sagittal schematic and photomicrograph of a coronal section showing the position of the microdialysis probe and cannula in the vCA1, and protocol for experiments I and J. Scale bar: 1 mm. (I and J) Microdialysis assay showed that blockade of Cx43 by Gap27 significantly suppressed CION-induced increases in extracellular ATP (I) and adenosine (J) in the vCA1. (K) Sagittal schematic and photomicrograph of a coronal section showing hM4Di or mCherry on vCA1 astrocytes, the position of the microdialysis probe in the vCA1, and the protocol for experiments M and N. (L) Double immunofluorescence staining revealed that GfaABC1D-mCherry was co-expressed with GFAP-IR, but not NeuN (a neuron marker)-IR, in the vCA1. Scale bar: 20 μm. (M and N) Chemogenetic inhibition of vCA1 astrocytes significantly decreased CION-induced upregulation of extracellular ATP (M) and adenosine (N) in the vCA1. Data are expressed as means ± SEM. *$p < 0.05$, **$p < 0.01$, two-tailed Student's *t*-test for B and E-G; two-way RM ANOVA followed by post hoc Sidak test for D; one-way ANOVA followed by post hoc Sidak test for I, J, M, and N. Sample sizes are indicated in bars and brackets.

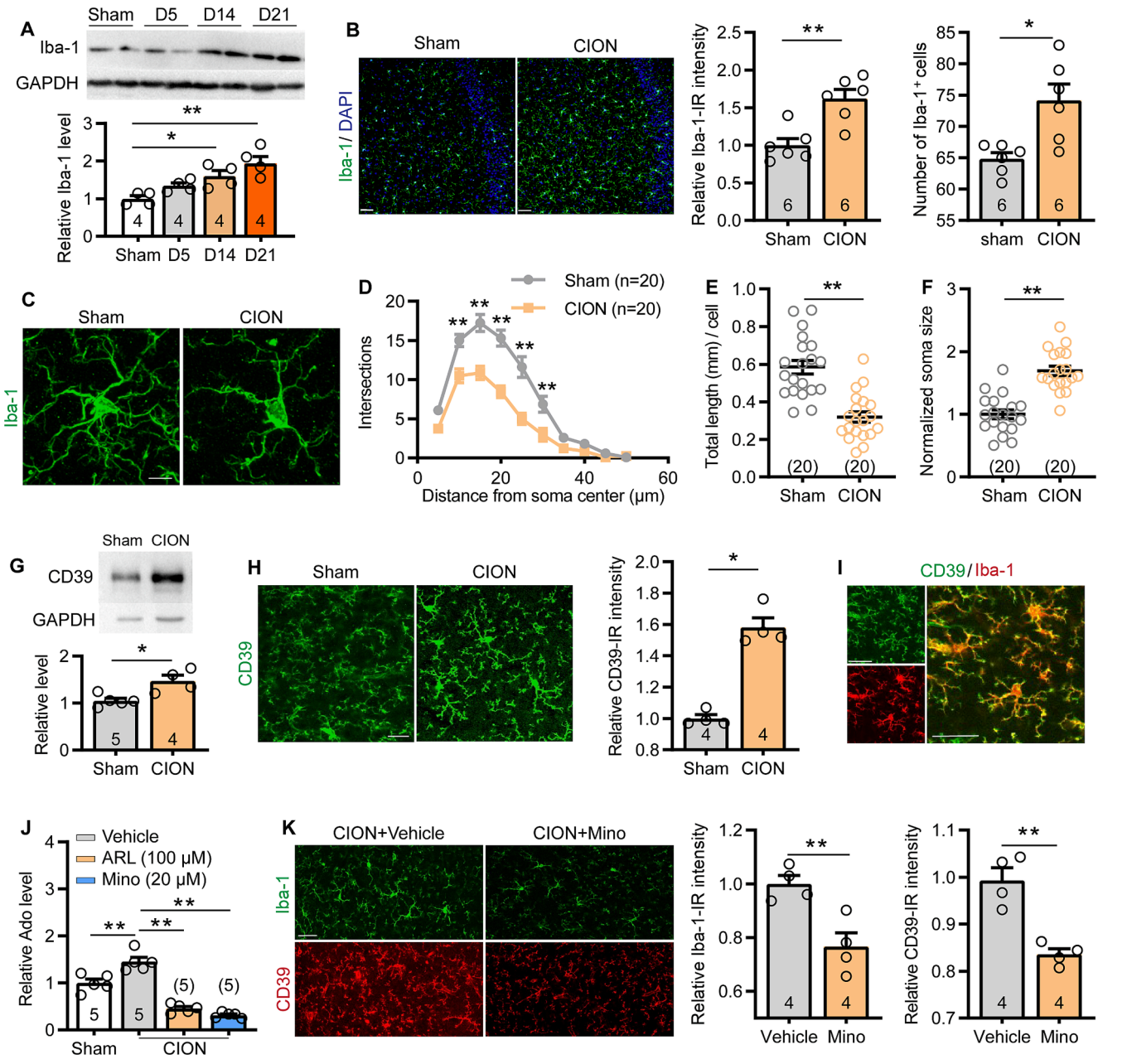

Fig. 3. Activated microglia and CD39 are involved in CION-induced increases in extracellular adenosine. (A) Western blot analysis revealed significant upregulation of Iba-1 (microglial marker) on days 14 and 21, but not day 5, after CION in the vHPC. (B) Immunofluorescence labeling revealed microglial activation, as indicated by increases in Iba-1 immunofluorescence and the number of ionized calcium-binding adaptor molecule (Iba)-1-positive cells in the vCA1. Scale bar: 50 μm. (C–F) Sholl analysis revealed shortened branches and enlarged soma in vCA1 microglia on day 14 after CION. Scale bar: 5 μm. (G) Western blot analysis revealed significant upregulation of CD39 on day 14 after CION. (H) Immunofluorescence staining of CD39 revealed increased CD39-IR in the vCA1 on day 14 after CION. Scale bar: 20 μm. (I) Double immunofluorescence staining revealed colocalization of CD39-IR and Iba-1-IR. Scale bar: 30 μm. (J) Microdialysis showed that inhibition of CD39 and microglia by ARL 67156 (ARL) and minocycline (Mino), respectively, significantly decreased CION-induced upregulation of extracellular adenosine in the vCA1. (K) Intraperitoneal injection of minocycline (50 mg/kg) efficiently suppressed Iba-1 and CD39 expression in the vCA1. Scale bar: 30 μm. Data are expressed as means ± SEM. *p < 0.05, **p < 0.01, two-tailed Student's *t*-test for B, E-G, and K; two-way RM ANOVA followed by post hoc Sidak test for D; one-way ANOVA followed by post hoc Sidak test for J. Sample sizes are indicated in bars and brackets.

2010). Thus, we further examined the effect of IL-17A on ATP release from astrocytes in the vCA1. We expressed genetically-encoded fluorescent GRABATP1.0 in vCA1 astrocytes (Wang et al., 2021; Wu et al., 2022). ATP sensor fluorescence intensity was measured after ex vivo sectioning. IL-17A induced a considerable increase in ATP1.0 fluorescence signal in vCA1 in the presence of TTX. Pretreatment of a reversible astrocytic metabolic inhibitor fluorocitrate (FC, 10 μM) or Gap27 inhibitor (100 μM) robustly reduced IL-17A-evoked ATP1.0 fluorescence intensity (Fig. 4E, I-N). To verify that the ATP1.0 in vCA1 astrocytes works efficiently in the presence of FC, we used ATP as a positive control. ATP (100 μM)-induced ATP1.0 fluorescence intensity was not influenced by FC (Supplementary Fig. 6E–H). A similar increase in adenosine sensor (Ado_B10) fluorescence intensity was observed in vCA1 neurons following IL-17A stimulation, which was completely blocked by the CD39 inhibitor ARL 67156 (100 μM, Supplementary Fig. 6I–K). These findings suggest that microglia promote astrocytic activation and ATP release through IL-17A.

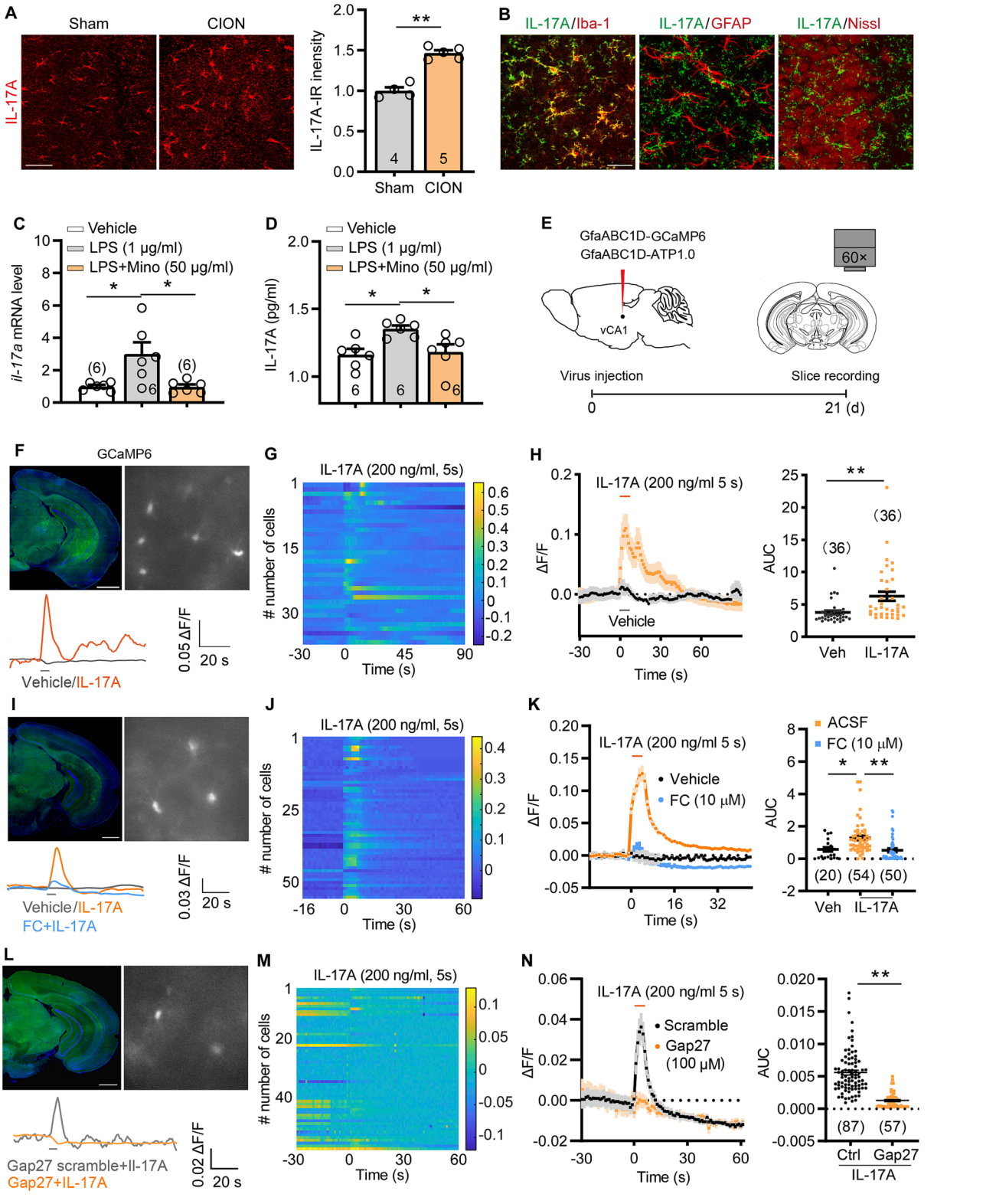

(caption on next page)

Fig. 4. CION upregulates interleukin (IL)-17A in vCA1 microglia, which promotes ATP release from astrocytes. (A) Immunofluorescence staining revealed an increase in IL-17A-IR in the vCA1 on day 14 after CION. Scale bar: 50 μm. (B) Double immunofluorescence staining showed that IL-17A-IR was mainly colocalized with Iba-1-IR, to a lesser extent with GFAP-IR, and not at all with Nissl-IR (a neuronal marker). Scale bar: 30 μm. (C) Real-time PCR showed that the *il-17a* mRNA level was elevated in lipopolysaccharide (LPS)-stimulated BV2 microglia, which was attenuated by a microglial inhibitor. (D) Enzyme-linked immunosorbent assay revealed that inhibition of microglia by minocycline blocked the LPS-induced increase of IL-17A in cultured medium of BV2 microglia. (E) Schematic of sagittal and coronal sections showing specific infection of GCaMP6 or ATP1.0 (an ATP sensor) on vCA1 astrocytes and the protocol for experiments F–N. (F) vHPC slice showing cells expressing GCaMP6 (upper) and representative calcium imaging of individual cells challenged by IL-17A (bottom). Scale bar: 1 mm. (G and H) The heat map of fluorescence (G), mean fluorescence of Ca^{2+} transients and AUC values of changes in Ca^{2+} transients (H) indicated a robust increase in the activity of vCA1 astrocytes following IL-17A treatment. During the recording of glial calcium signals, tetrodotoxin (TTX, 0.5 μM) and a cocktail of neurotransmitter receptor antagonists were added to the perfusate to exclude any influence of neurons. (I) vHPC slice image showing the recorded cells expressing ATP1.0 (upper) and representative images of individual cells challenged by IL-17A with and without fluorocitrate (FC; bottom). Scale bar: 1 mm. (J and K) The heat of fluorescence (J), mean fluorescence of ATP transients and AUC values of changes in ATP transients (K) indicated that IL-17A robustly increased extracellular ATP, although this was attenuated by the astrocytic metabolic inhibitor FC. (L) Representative images of individual cells challenged by IL-17A with Gap27 or Gap27 scramble. Scale bar: 1 mm. (M and N) The heat map of fluorescence (M), mean fluorescence of ATP transients and AUC values of changes in ATP transients (N) indicated that the Cx43 inhibitor Gap27 blocked IL-17A-induced ATP transients in vCA1 slices. Data are expressed as means ± SEM. *$p < 0.05$, **$p < 0.01$, two-tailed Student's *t*-test for A and H; one-way ANOVA followed by post hoc Sidak test for C, D, K, and N. Sample sizes are indicated in bars and brackets.

3.5. Inhibition of vCA1 microglia and CD39 alleviates CION-induced anxiodepressive-like behaviors

To achieve selective control of microglial activity, we crossed CX3CR1-CreER mice, harboring a tamoxifen (TAM)-inducible Cre recombinase with Ai35 mice carrying floxed stop-Arch-enhanced green fluorescent protein (EGFP) gene in the ROSA26 locus to generate CX3CR1-GFP::Arch mice. The optic fiber was implanted in the vCA1, and continuous yellow light (580 nm, 5 mW, 1 h/day) illumination was applied between days 14 and 22 after CION (Fig. 5A, B). Arch-EGFP signals were exclusively colocalized with Iba-1-IR after TAM injection, and yellow light stimulation significantly suppressed CION-induced microglial activation in the vCA1 (Fig. 5C). Optogenetic inhibition of vCA1 microglia markedly reversed CION-induced anxiodepressive-like behaviors in the EPM and TS tests (Fig. 5D, E). There was no difference between the two groups in closed arm entries in the EPM test, indicating that the phenotypic differences were not due to hyperactivity caused by yellow light-stimulation (Fig. 5D). Optogenetic inhibition of vCA1 microglia had no affect on CION-induced mechanical allodynia (Fig. 5F). The anti-anxiodepressive effect of inhibiting vCA1 microglia was further confirmed using a pharmacological approach. Intra-vCA1 injection of the microglial inhibitor minocycline (10 nmol) significantly suppressed CION-induced anxiodepressive-like behaviors (Fig. 5G-I). Similarly, the microglial CD39 inhibitor ARL 67156 (15 nmol) exhibited markedly anti-anxiodepressive effects in the EPM and TS tests (Fig. 5G, J and K). Minocycline and ARL 67156 injections the vCA1 had no effect on CION-induced mechanical allodynia (Fig. 5L and M). We also examined the effects of optogenetic activation of vCA1 microglia on CION-induced anxiodepressive-like behaviors. We crossed CX3CR1-CreER and floxed channelrhodopsin-2 (ChR2) mice to generate CX3CR1-GFP::ChR2 mice. ChR2-EGFP signals were exclusively colocalized with Iba-1-IR after TAM injection, and blue light (473 nm, 5 mW, 20 Hz, 30 min/day) illumination markedly activated of microglia in the vCA1 of CX3CR1-GFP::ChR2 mice (Supplementary Fig. 7A–D). Optogenetic activation of vCA1 microglia did not affect CION-induced anxiodepressive-like behaviors or allodynia (Supplementary Fig. 7E–G). Taken together, these results suggest that inhibiting vCA1 microglia, microglia-derived CD39, and IL-17A effectively alleviates CION-induced anxiodepressive-like behaviors by blocking ATP conversion into adenosine.

3.6. Inhibition of vCA1 astrocytes and Cx43 improves CION-induced anxiodepressive-like behaviors

To selectively control astrocytic activity, we injected AAV-encoding eNpHR virus (driven by the astrocyte-specific promoter) into the vCA1 area in CION mice; and GFAP-EGFP signals were colocalized with GFAP-IR almost without exception (Fig. 6A). Electrophysiological recording showed that yellow light stimulation of eNpHR-expressing astrocytes induced hyperpolarization in current-clamp modes (Fig. 6B and C). In particular, yellow light (580 nm, 5 mW, continuous) treatment effectively suppressed CION-induced astrocytic activation in the vCA1 (Fig. 6D). Behaviorally, optogenetic inhibition of vCA1 astrocytes blocked CION-induced anxiodepressive-like behaviors but did not affect mechanical allodynia (Fig. 6E and F; Supplementary Fig. 8A). Moreover, chemogenetic inhibition of vCA1 astrocytes expressing Gi-coupled hM4D receptors improved anxiodepressive-behaviors in rTN mice without mechanical allodynia (Fig. 6G-K, Supplementary Fig. 8B). Intra-vCA1 injection of L-2-aminoadipic acid (LAA, 6 nmol), an astrocyte cytotoxin, produced similar effects (Supplementary Fig. 8C–H). We also examined the effects of optogenetic activation of vCA1 astrocytes on CION-induced anxiodepressive-like behaviors. Similar to the effect of optogenetic activation of microglia, photoactivation of vCA1 astrocytes had no effect on CION-induced anxiodepressive-like behaviors or allodynia (Supplementary Fig. 9A-G).

Considering that blockade of Cx43 markedly reduced the extracellular ATP/adenosine level in the vHPC (Fig. 2I and J), we further examined the effect of a Cx43 blocker on CION-induced anxiodepressive-like behaviors. Intra-vCA1 of Gap27 (4 nmol), but not Gap-27 scramble, effectively alleviated anxiodepressive-like behaviors in rTN mice (Fig. 6L-N). Collectively, these data indicate that inhibiting astrocytic activation and Cx43 may produce anti-anxiodepressive effects by blocking the release of ATP from vCA1 astrocytes.

3.7. Blockade of A2AR and inhibition of glial activation normalizes CION-induced hyperexcitability of vCA1 pyramidal neurons

Increased excitability of CA1 pyramidal neurons in the vHPC is related to anxiodepressive-like behaviors (Fee et al., 2020; Jimenez et al., 2018). Our unpublished data showed that inhibition of CaMK2A-positive pyramidal neurons in the vCA1 effectively ameliorated CION-induced anxiodepressive-like behaviors. Here, we further confirmed that the excitability of vCA1 pyramidal neurons significantly increased on day 14 after CION. Whole-cell patch-clamp recordings were performed in vHPC slices, and action potentials were evoked by depolarizing current pulses of 0–200 pA (10-pA increments). The input–output curves were left-shifted at 14 days after CION (Fig. 7A and B). The A2AR antagonist DMPX (10 μM) significantly suppressed the neuronal activity of vCA1 pyramidal neurons (Fig. 7C and D). Intriguingly, bath of exogenous adenosine (2 μM) partially mimicked CION-induced hyperactivity of vCA1 pyramidal neurons, although this was blocked by DMPX pretreatment (Fig. 7E and F). Moreover, the CD39 inhibitor ARL (100 μM) and microglial inhibitor Mino (5 μM), as well as the astrocytic cytotoxin LAA (6 nmoL into vCA1 in vivo), reversed the excitability of vCA1 pyramidal neurons in rTN mice (Fig. 7G-L). Taken together with our previous data, these results suggest that the activation of glia and upregulation of extracellular adenosine induced by CION may mediate anxiodepressive-like behaviors by increasing the excitatory activity of

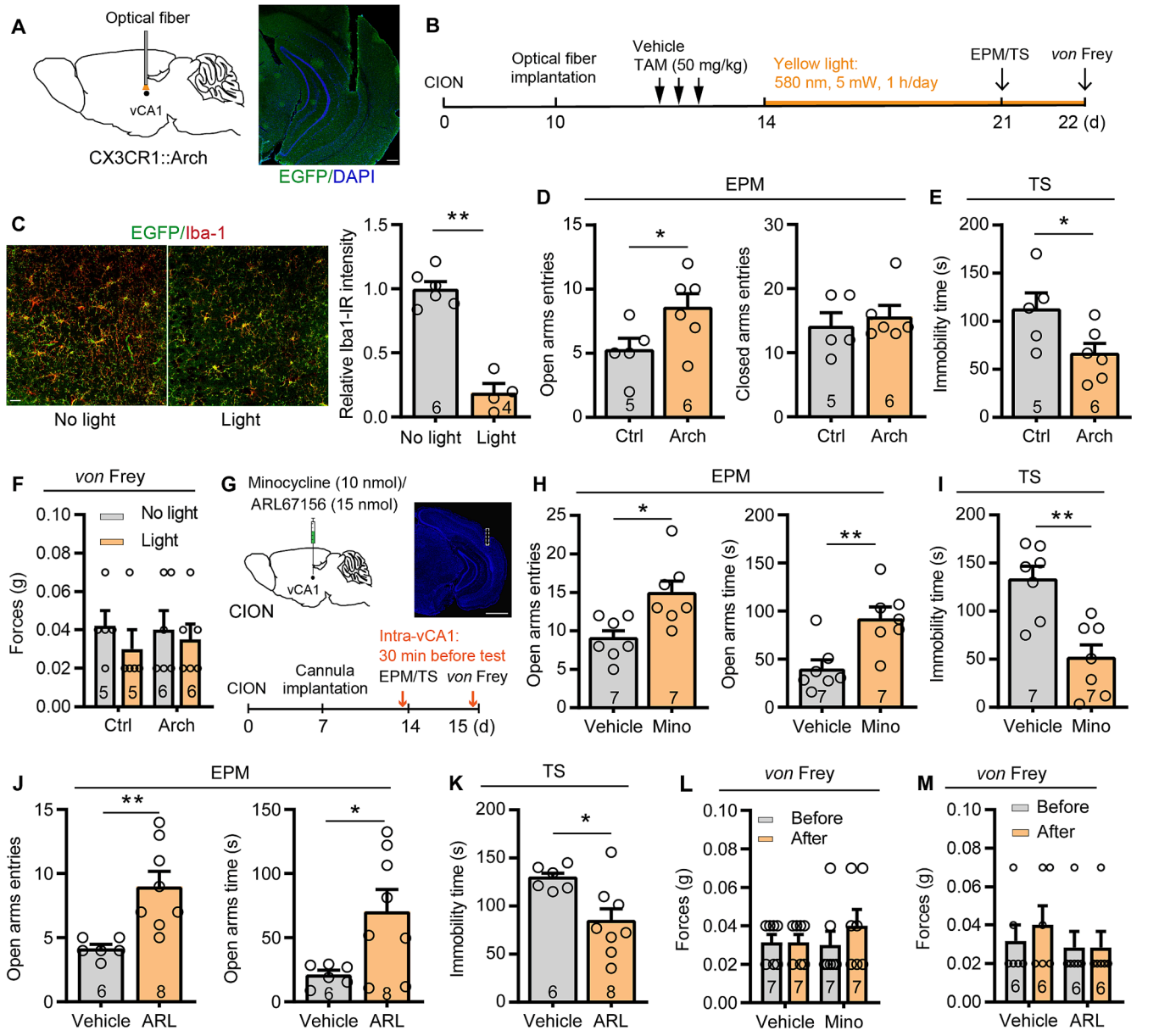

Fig. 5. Inhibition of vCA1 microglia and CD39 ameliorates CION-induced anxiodepressive-like behaviors. (A) Sagittal schematic and photomicrograph of a coronal section showing the site of optical fiber implantation in the vCA1 area of CX3CR1::Arch mice. Scale bar: 200 μm. (B) Schematic of the protocol for experiments C–E. (C) Double immunofluorescence staining revealed that Arch-enhanced green fluorescent protein (EGFP) was co-expressed with Iba-1 in the vCA1, and Iba-1-IR was reduced by continuous yellow light (580 nm, 5 mW). Scale bar: 20 μm. (D and E) Optogenetic inhibition of vCA1 microglia prevented anxiodepressive-like behaviors in the EPM (D) and TS (E) tests in CX3CR1::Arch mice. (F) Optogenetic inhibition of vCA1 microglia did not affect CION-induced mechanical allodynia. (G) Sagittal schematic and photomicrograph of a coronal section showing the cannula position and drug injection site in the vCA1, and the protocol for experiments H–M. Scale bar: 1 mm. (H–M) Intra-vCA1 injection of the microglial inhibitor minocycline or CD39 inhibitor ARL significantly alleviated CION-induced anxiodepressive-like behaviors in the EPM and TS tests, but did not affect mechanical allodynia in the *von* Frey test. Data are expressed as means ± SEM. *p < 0.05, **p < 0.01, two-tailed Student's *t*-test for D, E, H-K; two-way ANOVA for F, L, and M. Sample sizes are indicated in bars. (For interpretation of the references to colour in this figure legend, the reader is referred to the web version of this article.)

vCA1 pyramidal neurons.

4. Discussion

Accumulating evidence suggests that microglial and astrocytic activity is crucial for purinergic signal regulation, which is believed to be involved in the comorbid mechanisms of depression and chronic pain (Zou et al., 2023). Our recent study demonstrated the essential role of microglial P2X7 receptor signaling in neuropathic pain and depression (Chen et al., 2023). In the present study, we further revealed that persistent pain activates microglia and astrocytes in the vCA1, upregulates extracellular ATP/adenosine expression, and increases the neuronal activity of vCA1 pyramidal neurons through A2AR, which may explain the observed anxiodepressive-like effects (Fig. 8). Our findings provide deeper insight into the functional consequences of microglia-astrocyte crosstalk.

4.1. Activation of microglia and astrocytes in the vCA1 is involved in the pathogenesis of neuropathic pain and anxiodepression

Human studies have demonstrated a role for neuroinflammation in affective disorders (Benatti et al., 2016; Klawonn et al., 2021; Najjar

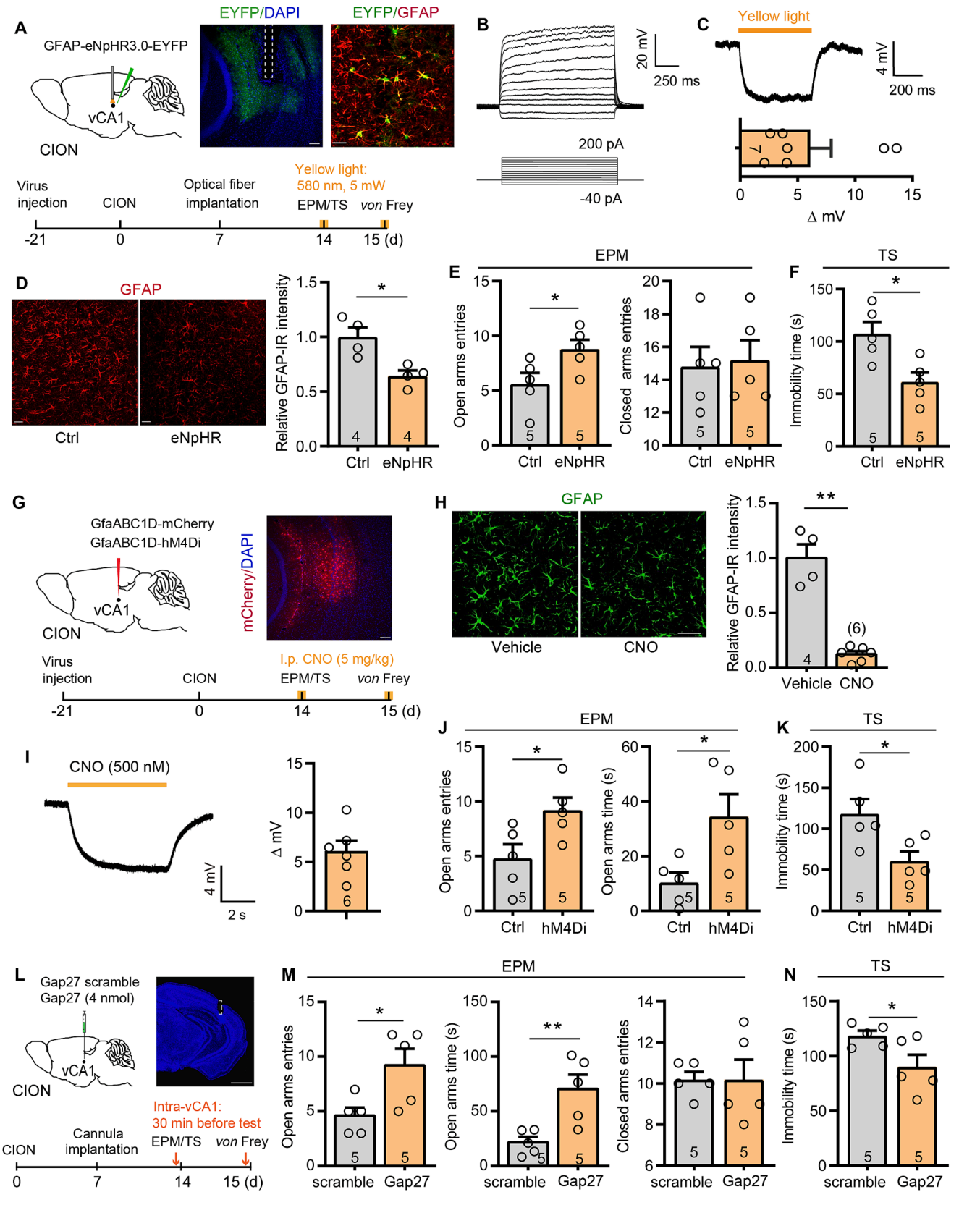

(caption on next page)

Fig. 6. Inhibition of vCA1 astrocytes and Cx43 alleviates CION-induced anxiodepressive-like behaviors. (A) Sagittal schematic and photomicrograph of coronal section showing GFAP-eNpHR3.0 or mCherry on vCA1 astrocytes and the location of optical fiber implantation in the vCA1, and protocol for experiments E and F. Scale bar: 200 μm (left); 20 μm (right). (B) A typical non-excitable response of astrocyte to step current stimulation in current-clamp mode. (C) Yellow light stimulation (580 nm) of eNpHR-expressing astrocytes induced hyperpolarization in current-clamp mode. (D) GFAP-IR of the vCA1 was reduced by continuous yellow light (580 nm, 5 mW). Scale bar: 20 μm. (E and F) Optogenetic inhibition of vCA1 astrocytes alleviated CION-induced anxiodepressive-like behaviors in the EPM (E) and TS (F) tests. (G) Sagittal schematic and photomicrograph of a coronal section showing GfaABC1D-hM4Di or mCherry on vCA1 astrocytes, and protocol for experiments J and K. Scale bar:200 μm. (H) Chemogenetic inhibition of vCA1 astrocytes significantly decreased GFAP-IR. Scale bar: 30 μm. (I) Puff application of CNO hyperpolarized membrane potential of hM4Di-expressing astrocyte. (J and K) Chemogenetic inhibition of vCA1 astrocytes significantly ameliorated CION-induced anxiodepressive-like behaviors in the EPM (J) and TS (K) tests. (L) Sagittal schematic and photomicrograph of a coronal section showing the site of drug injection and cannula location in the vCA1, and the protocol for experiments M and N. Scale bar: 1 mm. (M and N) Intra-vCA1 injection of the Cx43 inhibitor Gap27 alleviated CION-induced anxiodepressive-like behaviors. Data are expressed as means ± SEM. *p < 0.05, **p < 0.01, two-tailed Student's *t*-test. Sample sizes are indicated in bars. (For interpretation of the references to colour in this figure legend, the reader is referred to the web version of this article.)

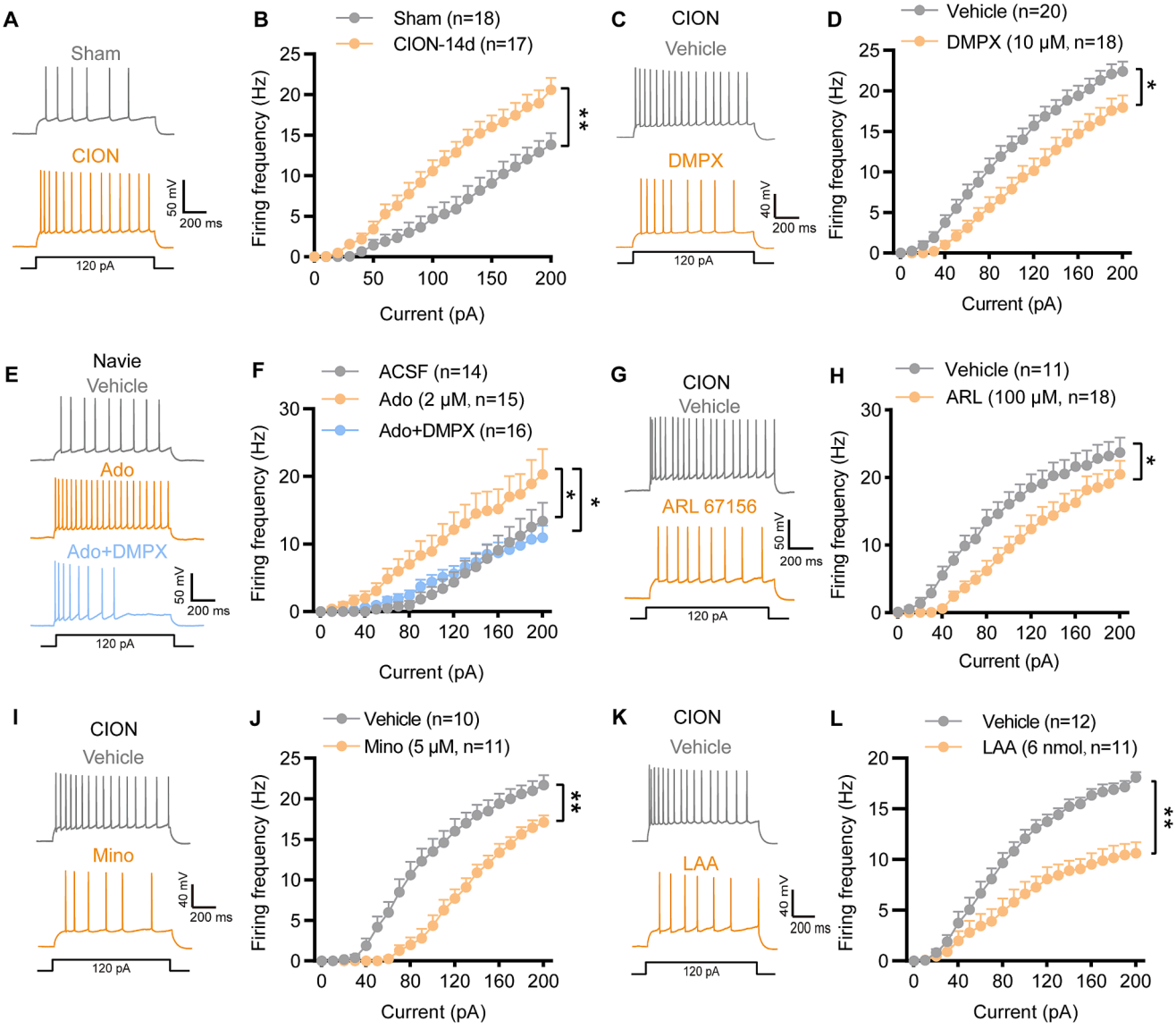

Fig. 7. Effects of blocking A2AR or inhibiting glial activation on the excitability of vCA1 pyramidal neurons in CION mice. (A) Current clamp recording action potentials (APs) evoked by depolarizing current pulses in vCA1 pyramidal neurons from sham- and 14-day-CION mice. (B) CION increased the firing frequency of APs evoked by depolarizing current pulses in vCA1 pyramidal neurons on day 14. (C and D) Perfusion of the A2AR antagonist DMPX reversed the increase in firing frequency of APs induced by CION. (E and F) Adenosine increased the firing frequency of APs, although this was blocked by the A2AR antagonist DMPX. (G–L) Inhibition of CD39 (ARL; G and H), microglia (Mino; I and J), and astrocytes (L-2-aminoadipic acid [LAA]; K and L) reversed the increased firing frequency of APs induced by CION. Data are expressed as means ± SEM. *p < 0.05, **p < 0.01, two-way RM ANOVA. Sample sizes are indicated in brackets.

et al., 2013). The onset and progression of chronic pain is also strongly associated with the inflammatory response (Chen et al., 2018; Ji et al., 2016). In the central nervous system (CNS), microglia and astrocytes are the two major sources of innate immunity. Increased glial activation and production of inflammatory mediators in mood-related brain areas has been observed in chronic pain patients (Loggia et al., 2015; Perry et al., 2016) and animal models (Cui et al., 2020b; Ghaemi et al., 2018; Sutulovic et al., 2023). In experimental chronic prostatitis/chronic

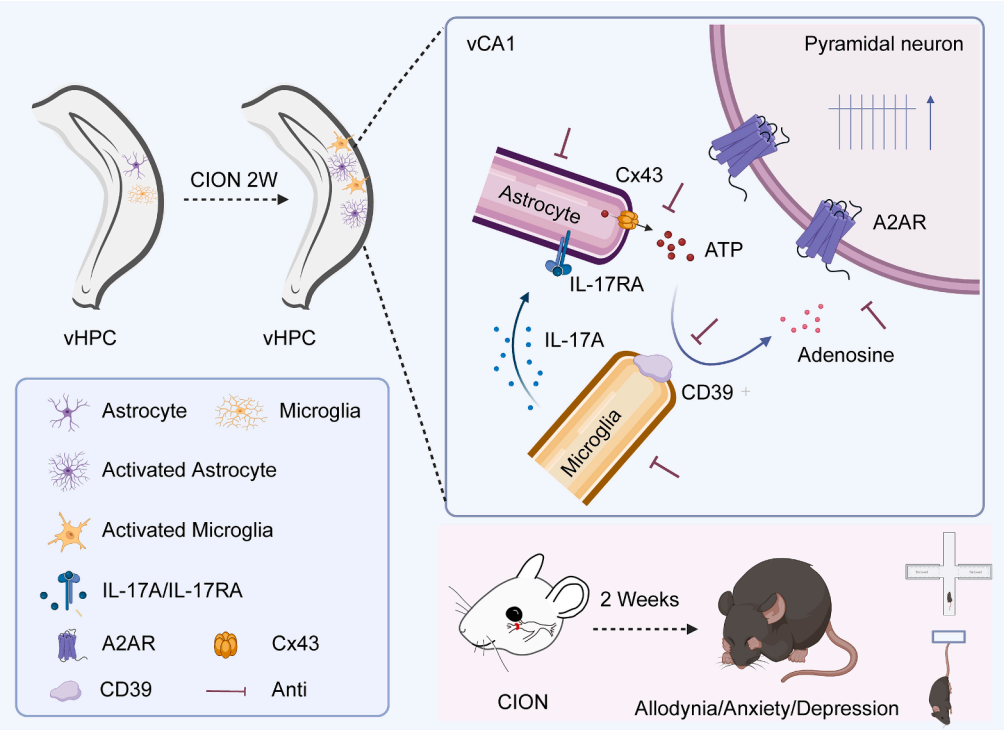

Fig. 8. Schematic showing the potential mechanisms through which vHPC glia-derived adenosine drives the anxiodepressive-like behaviors in a mouse model resembling trigeminal neuralgia. CION increases extracellular adenosine levels by activating vCA1 astrocytes and microglia. Activated astrocytes release excessive ATP, which is converted into adenosine by microglial CD39 and thereby enhances the excitability of vCA1 pyramidal neurons via A2AR. Inhibiting vCA1 astrocytic and microglial activation, attenuating the conversion of ATP into adenosine, and blocking A2AR can all improve pain-related anxiety and depression.

pelvic pain syndrome (Du et al., 2019; Sutulovic et al., 2023) and neuropathic pain (Cui et al., 2020b; Manzhulo et al., 2021) models, increased expression of both Iba-1-IR and GFAP-IR was observed in the hippocampus.

The hippocampus is a heterogeneous structure with functional differences along the dorsoventral axis, and the ventral hippocampus (vHPC) is considered important for emotional regulation (Strange et al., 2014). In a nonhuman primate model of anxious temperament, high-resolution fluorodeoxyglucose-positron emission tomography revealed increased metabolic activity in the anterior hippocampus (analogous to the vHPC in rodents (Shackman et al., 2013). A recent study showed that vCA1 pyramidal neuronal activity was also modulated by nociceptive stimulation (Wang et al., 2023). In a rat model of neuropathic pain, neuroimmune activation in the vHPC coincided with affective behavioral changes in susceptible individuals, regardless of the strength of nociceptive responses (Fiore and Austin, 2019). The current study provides new evidence that activation of microglia and astrocytes in the vHPC is crucial for the anxiodepressive-like consequences of neuropathic pain. The activation of microglia and astrocytes in the vHPC induced by CION is time dependent, and the time window of vHPC glial activation coincides with the development of anxiodepressive-like behaviors after CION. More importantly, we found that inhibition of either microglia or astrocytes in the vHPC reversed CION-induced hyperexcitability of vHPC pyramidal neurons and anxiodepressive-like behaviors. In support of the present results, increased neuronal activation and inflammatory processes in the vHPC were also closely related to vulnerability to social stress (Pearson-Leary et al., 2017) and chronic stress plus social isolation (Du Preez et al., 2021).

It should be mention that recent reports highlighted a sex specific difference in the immune-driven tactile allodynia in neuropathic pain (Boccella et al., 2019; Luo et al., 2021; Mapplebeck et al., 2017; Sorge et al., 2015; Tu et al., 2022). For example, in spinal nerve injury (SNI)-induced mouse neuropathic pain, spinal microglia and Toll-like receptor 4 (TLR4), specifically expressed on microglia in the CNS, mainly contribute to the mechanical hyperalgesia of male mice rather than female mice (Sorge et al., 2011; Sorge et al., 2015). Inhibition of spinal p38 MAP kinase alleviated neuropathic pain in male but not female mice (Taves et al., 2016). However, whether the sexual dimorphism extends to glia in supraspinal level was hitherto untested. In the present study, we did not find the difference between male and female mice in pain-related anxiodepressive-like behaviors and vHPC glial responses after CION, providing universal targets for therapeutic strategies against anxiodepressive consequences of chronic pain for both sexes.

4.2. Astrocytes and microglia synergistically regulate extracellular ATP/adenosine level in the vCA1

Astrocytes perform numerous critical functions such as formation of the blood–brain barrier, regulation of extracellular ion concentrations, neurotransmitter recycling, and modulation of synaptic transmission. Following nerve injury or disease, astrocytes lose their ability to maintain the homeostatic concentrations of extracellular ions and neurotransmitters, leading to neuronal hyperexcitability (Ji et al., 2016). Cx43 is the predominant connexin expressed in astrocytes, mediating gap junction communication. Persistent activation of astrocytes may lead to a change in function of Cx43 from gap junction communication to paracrine modulation, in turn increasing the release of gliotransmitters such as ATP (Chen et al., 2014; Hamilton and Attwell, 2010; Torres et al., 2012). In the present study, we observed a significant increase in Cx43 in the vHPC astrocytes of rTN mice. Blockade of Cx43 suppressed CION-induced upregulation of extracellular ATP/adenosine in the vHPC and anxiodepressive-like behaviors. Furthermore, silencing vHPC astrocytes also effectively reduced extracellular ATP/adenosine expression and CION-induced anxiodepressive-like behaviors. Stimulation of vHPC astrocytes by IL-17A rapidly increased ATP and adenosine signaling. Our data suggest that the upregulation of ATP/adenosine in the vHPC of rTN mice may primarily be caused by astrocytes.

As mentioned above, the ATP released by astrocytes is the main

source of extracellular adenosine. Extracellular adenosine levels are regulated by the astroglia-based adenosine cycle, and enzymes that degrade ATP into adenosine outside the cell include two ecto-enzymes, CD39 and CD73. Extracellular ATP is hydrolyzed into AMP by CD39 and then is hydrolyzed into adenosine by CD73 (Liu et al., 2019; Moesta et al., 2020). As an apical and rate-limiting ecto-enzyme involved in this process, CD39 plays a crucial role in maintaining extracellular adenosine homeostasis (Moesta et al., 2020). In the current study, we observed increased CD39 expression in vHPC microglia of rTN mice, although this was attenuated by a microglial inhibitor. In particular, inhibition of either CD39 or microglia significantly reduced extracellular adenosine and relieved CION-induced anxiodepression. In support of this, it has been reported that the expression and activity of CD39 in the hippocampus were enhanced by chronic social defeat stress; pharmacological inhibition and genetic silencing of CD39 produced antidepressant-like effects by increasing the extracellular hippocampal ATP concentration (Cui et al., 2020a).

Microglia, as the resident macrophages in the spinal cord and brain, are a heterogeneous population throughout the CNS. They sense the cellular environment with their ramified processes and undergo rapid morphological changes in response to mediators such as ATP (Chen et al., 2018; Davalos et al., 2005). Activated microglia prompt the overproduction of several pro-inflammatory mediators, such as TNF-α, IL-1β, and IL-18, which contribute to the development of chronic pain and depression (Chen et al., 2023; Yang et al., 2015). We found that mRNA and protein IL-17A expression was significantly upregulated in the vHPC of rTN mice. Moreover, it has been reported that the microglia express IL-17A in the brain after cerebral ischemia reperfusion (Kawanokuchi et al., 2008; Shichita et al., 2012). Consistent with this, we observed that IL-17A was mainly co-labeled with Iba-1-IR in rTN mice. LPS stimulation increased IL-17A mRNA expression in BV2 microglia and IL-17A release in BV2 culture medium, although this was blocked by minocycline treatment. Astrocytes are assumed to be one of the main targets of IL-17A signaling (Gelderblom et al., 2012). Indeed, we found that, in vHPC slices IL-17A selectively increased astrocytic intracellular calcium and extracellular ATP/adenosine signaling. Collectively, these results indicate that activated microglia and astrocytes synergistically contribute to the upregulation of extracellular ATP/adenosine in the vCA1 after CION.

The effect of extracellular adenosine on brain function is mainly depends on the activity of high affinity adenosine A1R and A2AR, which are widely distributed in the brain and implicated in mood regulation (Camargo et al., 2023). For example, human A2AR gene polymorphisms are associated with the incidence and clinical heterogeneity of depression (Moreira-de-Sa et al., 2021). Mice exposed to chronic unpredictable stress (Kaster et al., 2015) and helpless stress (Machado et al., 2017) displayed higher A2AR density in hippocampal synapses. Genetic deletion or pharmacological blockade of A2AR attenuated various depressive-like behaviors (Dai et al., 2010; Rebola et al., 2011). Similarly, in a mouse model of chronic pain we found that pharmacological or genetic blockade of vHPC A2AR but not A1R ameliorated anxiodepressive-like behaviors and reversed the vHPC neuronal hyperexcitability induced by CION. Directly administering an A2AR antagonist directly had the same effect as silencing astrocytes and microglia themselves. These findings indicated that ATP/adenosine and adenosine A2AR were responsible for the anxiodepressive-like effects of rTN.

4.3. Translational potential and limitations

We found that selective silencing of vHPC microglia and astrocytes, and inhibition of CD39, IL-17A, Cx43, and A2AR, effectively alleviated CION-induced anxiodepression (Fig. 8). Therefore, targeting vHPC glia and their products may have therapeutic potential for emotional disorders caused by chronic pain.

This study also had some limitations. For example, hippocampal astrocyte atrophy and decreased GFAP expression have been observed in postmortem brain samples from suicide depressed patients (Cobb et al., 2016) and in animal models of depression (Czeh et al., 2006; Gong et al., 2012; Zhao et al., 2018). By contrast, our results showed that vHPC astrocytes were robustly activated 2 weeks after CION. Whether vHPC astrocytes transition from activation to atrophy during the development of chronic pain remains unclear. Further study on the dynamic process of astrocytic activity in different stages of chronic pain development will be important to understand the pathogenesis of pain-related anxiodepression. In addition, astrocytes secrete ATP through several major pathways that do not involve Cx43 connexin (Torres et al., 2012). Further studies of other ATP release pathways, such as Ca^{2+}-dependent exocytosis via the lysosomal pathway, implicated in chronic pain-induced anxiodepression are needed.

5. Authors' contributions

X.J. Lv and Y.Q. Zhang designed the experiments. Y.Q. Zhang, W.D. Xu, and G. Xu conceived the project. X.J. Lv performed surgery, behavioral tests, immunohistochemistry, western blotting experiments, intra-vCA1 injection of virus stereotaxic injection and chemogenetic and optogenetic manipulation. S.S. Lv performed electophysiological recording and participated the optogenetic manipulation and behavioral experiments. G.H. Wang participated in fiber photometry and behavioral experiments. Y. Chang participated in immunohistochemical and western blotting experiments. X.J. Lv and Y.Q. Zhang analyzed the data and wrote the manuscript. All the authors read and discussed the manuscript.

Declaration of competing interest

The authors declare that they have no known competing financial interests or personal relationships that could have appeared to influence the work reported in this paper.

Data availability

All data needed to evaluate the conclusions in the paper are present in the paper and/or the Supplementary Materials.

Acknowledgments

This work was supported by National Natural Science Foundation of China (31930042, 82130032, and 82021002); STI 2030-Major Projects (2021ZD0203200-5), Shanghai Municipal Science and Technology Major Project (No.2018SHZDZX01), ZJLab and Shanghai Center for Brain Science and Brain-Inspired Technology, China.

Appendix A. Supplementary data

Supplementary data to this article can be found online at https://doi.org/10.1016/j.bbi.2024.01.012.

References

Araque, A., Carmignoto, G., Haydon, P.G., Oliet, S.H., Robitaille, R., Volterra, A., 2014. Gliotransmitters travel in time and space. Neuron 81, 728–739. https://doi.org/10.1016/j.neuron.2014.02.007.

Badimon, A., Strasburger, H.J., Ayata, P., Chen, X., Nair, A., Ikegami, A., Hwang, P., Chan, A.T., Graves, S.M., Uweru, J.O., Ledderose, C., Kutlu, M.G., Wheeler, M.A., Kahan, A., Ishikawa, M., Wang, Y.C., Loh, Y.E., Jiang, J.X., Surmeier, D.J., Robson, S. C., Junger, W.G., Sebra, R., Calipari, E.S., Kenny, P.J., Eyo, U.B., Colonna, M., Quintana, F.J., Wake, H., Gradinaru, V., Schaefer, A., 2020. Negative feedback control of neuronal activity by microglia. Nature 586, 417–423. https://doi.org/10.1038/s41586-020-2777-8.

Bartoli, F., Burnstock, G., Crocamo, C., Carra, G., 2020. Purinergic signaling and related biomarkers in depression. Brain Sci. 10 https://doi.org/10.3390/brainsci10030160.

Benatti, C., Blom, J.M., Rigillo, G., Alboni, S., Zizzi, F., Torta, R., Brunello, N., Tascedda, F., 2016. Disease-induced neuroinflammation and depression. CNS

Neurol. Disord. Drug Targets 15, 414–433. https://doi.org/10.2174/1871527315666160321104749.
Boccella, S., Guida, F., De Logu, F., De Gregorio, D., Mazzitelli, M., Belardo, C., Iannotta, M., Serra, N., Nassini, R., de Novellis, V., Geppetti, P., Maione, S., Luongo, L., 2019. Ketones and pain: unexplored role of hydroxyl carboxylic acid receptor type 2 in the pathophysiology of neuropathic pain. FASEB J. 33, 1062–1073. https://doi.org/10.1096/fj.201801033R.
Boison, D., Chen, J.F., Fredholm, B.B., 2010. Adenosine signaling and function in glial cells. Cell Death Differ. 17, 1071–1082. https://doi.org/10.1038/cdd.2009.131.
Camargo, A., Bettio, L.E.B., Rosa, P.B., Rosa, J.M., Alte, G.A., Rodrigues, A.L.S., 2023. The antidepressant-like effect of guanosine involves the modulation of adenosine A (1) and A(2A) receptors. Purinergic Signal 19, 387–399. https://doi.org/10.1007/s11302-022-09898-8.
Cao, X., Li, L.P., Wang, Q., Wu, Q., Hu, H.H., Zhang, M., Fang, Y.Y., Zhang, J., Li, S.J., Xiong, W.C., Yan, H.C., Gao, Y.B., Liu, J.H., Li, X.W., Sun, L.R., Zeng, Y.N., Zhu, X.H., Gao, T.M., 2013. Astrocyte-derived ATP modulates depressive-like behaviors. Nat. Med. 19, 773–777. https://doi.org/10.1038/nm.3162.
Chen, L.Q., Lv, X.J., Guo, Q.H., Lv, S.S., Lv, N., Xu, W.D., Yu, J., Zhang, Y.Q., 2023. Asymmetric activation of microglia in the hippocampus drives anxiodepressive consequences of trigeminal neuralgia in rodents. Br. J. Pharmacol. 180, 1090–1113. https://doi.org/10.1111/bph.15994.
Chen, G., Park, C.K., Xie, R.G., Berta, T., Nedergaard, M., Ji, R.R., 2014. Connexin-43 induces chemokine release from spinal cord astrocytes to maintain late-phase neuropathic pain in mice. Brain 137, 2193–2209. https://doi.org/10.1093/brain/awu140.
Chen, G., Zhang, Y.Q., Qadri, Y.J., Serhan, C.N., Ji, R.R., 2018. Microglia in Pain: Detrimental and Protective Roles in Pathogenesis and Resolution of Pain. Neuron 100, 1292–1311. https://doi.org/10.1016/j.neuron.2018.11.009.
Cobb, J.A., O'Neill, K., Milner, J., Mahajan, G.J., Lawrence, T.J., May, W.L., Miguel-Hidalgo, J., Rajkowska, G., Stockmeier, C.A., 2016. Density of GFAP-immunoreactive astrocytes is decreased in left hippocampi in major depressive disorder. Neuroscience 316, 209–220. https://doi.org/10.1016/j.neuroscience.2015.12.044.
Cui, S.S., Feng, X.B., Zhang, B.H., Xia, Z.Y., Zhan, L.Y., 2020b. Exendin-4 attenuates pain-induced cognitive impairment by alleviating hippocampal neuroinflammation in a rat model of spinal nerve ligation. Neural Regen. Res. 15, 1333–1339. https://doi.org/10.4103/1673-5374.272620.
Cui, Q.Q., Hu, Z.L., Hu, Y.L., Chen, X., Wang, J., Mao, L., Lu, X.J., Ni, M., Chen, J.G., Wang, F., 2020a. Hippocampal CD39/ENTPD1 promotes mouse depression-like behavior through hydrolyzing extracellular ATP. EMBO Rep. 21, e47857. http://doi.org/10.15252/embr.201947857.
Czeh, B., Simon, M., Schmelting, B., Hiemke, C., Fuchs, E., 2006. Astroglial plasticity in the hippocampus is affected by chronic psychosocial stress and concomitant fluoxetine treatment. Neuropsychopharmacology 31, 1616–1626. https://doi.org/10.1038/sj.npp.1300982.
Dai, S.S., Zhou, Y.G., Li, W., An, J.H., Li, P., Yang, N., Chen, X.Y., Xiong, R.P., Liu, P., Zhao, Y., Shen, H.Y., Zhu, P.F., Chen, J.F., 2010. Local glutamate level dictates adenosine A2A receptor regulation of neuroinflammation and traumatic brain injury. J. Neurosci. 30, 5802–5810. https://doi.org/10.1523/JNEUROSCI.0268-10.2010.
Davalos, D., Grutzendler, J., Yang, G., Kim, J.V., Zuo, Y., Jung, S., Littman, D.R., Dustin, M.L., Gan, W.B., 2005. ATP mediates rapid microglial response to local brain injury in vivo. Nat. Neurosci. 8, 752–758. https://doi.org/10.1038/nn1472.
Du, H.X., Chen, X.G., Zhang, L., Liu, Y., Zhan, C.S., Chen, J., Zhang, Y., Yu, Z.Q., Zhang, J., Yang, H.Y., Zhong, K., Liang, C.Z., 2019. Microglial activation and neurobiological alterations in experimental autoimmune prostatitis-induced depressive-like behavior in mice. Neuropsychiatr. Dis. Treat. 15, 2231–2245. https://doi.org/10.2147/NDT.S211288.
Du Preez, A., Onorato, D., Eiben, I., Musaelyan, K., Egeland, M., Zunszain, P.A., Fernandes, C., Thuret, S., Pariante, C.M., 2021. Chronic stress followed by social isolation promotes depressive-like behaviour, alters microglial and astrocyte biology and reduces hippocampal neurogenesis in male mice. Brain Behav. Immun. 91, 24–47. https://doi.org/10.1016/j.bbi.2020.07.015.
Duman, R.S., Aghajanian, G.K., 2012. Synaptic dysfunction in depression: potential therapeutic targets. Science 338, 68–72. https://doi.org/10.1126/science.1222939.
Fasick, V., Spengler, R.N., Samankan, S., Nader, N.D., Ignatowski, T.A., 2015. The hippocampus and TNF: Common links between chronic pain and depression. Neurosci. Biobehav. Rev. 53, 139–159. https://doi.org/10.1016/j.neubiorev.2015.03.014.
Fee, C., Prevot, T., Misquitta, K., Banasr, M., Sibille, E., 2020. Chronic Stress-induced Behaviors Correlate with Exacerbated Acute Stress-induced Cingulate Cortex and Ventral Hippocampus Activation. Neuroscience 440, 113–129. https://doi.org/10.1016/j.neuroscience.2020.05.034.
Fenn, A.M., Gensel, J.C., Huang, Y., Popovich, P.G., Lifshitz, J., Godbout, J.P., 2014. Immune activation promotes depression 1 month after diffuse brain injury: a role for primed microglia. Biol. Psychiatry 76, 575–584. https://doi.org/10.1016/j.biopsych.2013.10.014.
Fiore, N.T., Austin, P.J., 2019. Peripheral Nerve Injury Triggers Neuroinflammation in the Medial Prefrontal Cortex and Ventral Hippocampus in a Subgroup of Rats with Coincident Affective Behavioural Changes. Neuroscience 416, 147–167. https://doi.org/10.1016/j.neuroscience.2019.08.005.
Gelderblom, M., Weymar, A., Bernreuther, C., Velden, J., Arunachalam, P., Steinbach, K., Orthey, E., Arumugam, T.V., Leypoldt, F., Simova, O., Thom, V., Friese, M.A., Prinz, I., Holscher, C., Glatzel, M., Korn, T., Gerloff, C., Tolosa, E., Magnus, T., 2012. Neutralization of the IL-17 axis diminishes neutrophil invasion and protects from ischemic stroke. Blood 120, 3793–3802. https://doi.org/10.1182/blood-2012-02-412726.
Ghaemi, A., Alizadeh, L., Babaei, S., Jafarian, M., Khaleghi, G.M., Meuth, S.G., Kovac, S., Gorji, A., 2018. Astrocyte-mediated inflammation in cortical spreading depression. Cephalalgia 38, 626–638. https://doi.org/10.1177/0333102417702132.
Gong, Y., Sun, X.L., Wu, F.F., Su, C.J., Ding, J.H., Hu, G., 2012. Female early adult depression results in detrimental impacts on the behavioral performance and brain development in offspring. CNS Neurosci. Ther. 18, 461–470. https://doi.org/10.1111/j.1755-5949.2012.00324.x.
Hamilton, N.B., Attwell, D., 2010. Do astrocytes really exocytose neurotransmitters? Nat. Rev. Neurosci. 11, 227–238. https://doi.org/10.1038/nrn2803.
Hisaoka-Nakashima, K., Taki, S., Watanabe, S., Nakamura, Y., Nakata, Y., Morioka, N., 2019. Mirtazapine increases glial cell line-derived neurotrophic factor production through lysophosphatidic acid 1 receptor-mediated extracellular signal-regulated kinase signaling in astrocytes. Eur. J. Pharmacol. 860, 172539 https://doi.org/10.1016/j.ejphar.2019.172539.
Ji, R.R., Chamessian, A., Zhang, Y.Q., 2016. Pain regulation by non-neuronal cells and inflammation. Science 354, 572–577. https://doi.org/10.1126/science.aaf8924.
Jimenez, J.C., Su, K., Goldberg, A.R., Luna, V.M., Biane, J.S., Ordek, G., Zhou, P., Ong, S. K., Wright, M.A., Zweifel, L., Paninski, L., Hen, R., Kheirbek, M.A., 2018. Anxiety Cells in a Hippocampal-Hypothalamic Circuit. Neuron 97, 670–683.e676. https://doi.org/10.1016/j.neuron.2018.01.016.
Kang, J., Kang, N., Lovatt, D., Torres, A., Zhao, Z., Lin, J., Nedergaard, M., 2008. Connexin 43 hemichannels are permeable to ATP. J. Neurosci. 28, 4702–4711. https://doi.org/10.1523/JNEUROSCI.5048-07.2008.
Kaster, M.P., Machado, N.J., Silva, H.B., Nunes, A., Ardais, A.P., Santana, M., Baqi, Y., Muller, C.E., Rodrigues, A.L., Porciuncula, L.O., Chen, J.F., Tome, A.R., Agostinho, P., Canas, P.M., Cunha, R.A., 2015. Caffeine acts through neuronal adenosine A2A receptors to prevent mood and memory dysfunction triggered by chronic stress. PNAS 112, 7833–7838. https://doi.org/10.1073/pnas.1423088112.
Kawanokuchi, J., Shimizu, K., Nitta, A., Yamada, K., Mizuno, T., Takeuchi, H., Suzumura, A., 2008. Production and functions of IL-17 in microglia. J. Neuroimmunol. 194, 54–61. https://doi.org/10.1016/j.jneuroim.2007.11.006.
Kimura, L.F., Novaes, L.S., Picolo, G., Munhoz, C.D., Cheung, C.W., Camarini, R., 2022. How environmental enrichment balances out neuroinflammation in chronic pain and comorbid depression and anxiety disorders. Br. J. Pharmacol. 179, 1640–1660. https://doi.org/10.1111/bph.15584.
Klawonn, A.M., Fritz, M., Castany, S., Pignatelli, M., Canal, C., Simila, F., Tejeda, H.A., Levinsson, J., Jaarola, M., Jakobsson, J., Hidalgo, J., Heilig, M., Bonci, A., Engblom, D., 2021. Microglial activation elicits a negative affective state through prostaglandin-mediated modulation of striatal neurons. Immunity 54, 225–234. e226. https://doi.org/10.1016/j.immuni.2020.12.016.
Kol, A., Adamsky, A., Groysman, M., Kreisel, T., London, M., Goshen, I., 2020. Astrocytes contribute to remote memory formation by modulating hippocampal-cortical communication during learning. Nat. Neurosci. 23, 1229–1239. https://doi.org/10.1038/s41593-020-0679-6.
Lanser, A.J., Rezende, R.M., Rubino, S., Lorello, P.J., Donnelly, D.J., Xu, H., Lau, L.A., Dulla, C.G., Caldarone, B.J., Robson, S.C., Weiner, H.L., 2017. Disruption of the ATP/adenosine balance in CD39(-/-) mice is associated with handling-induced seizures. Immunology 152, 589–601. https://doi.org/10.1111/imm.12798.
Leng, L., Zhuang, K., Liu, Z., Huang, C., Gao, Y., Chen, G., Lin, H., Hu, Y., Wu, D., Shi, M., Xie, W., Sun, H., Shao, Z., Li, H., Zhang, K., Mo, W., Huang, T.Y., Xue, M., Yuan, Z., Zhang, X., Bu, G., Xu, H., Xu, Q., Zhang, J., 2018. Menin Deficiency Leads to Depressive-like Behaviors in Mice by Modulating Astrocyte-Mediated Neuroinflammation. Neuron 100, 551–563.e557. https://doi.org/10.1016/j.neuron.2018.08.031.
Liu, Y.J., Chen, J., Li, X., Zhou, X., Hu, Y.M., Chu, S.F., Peng, Y., Chen, N.H., 2019. Research progress on adenosine in central nervous system diseases. CNS Neurosci. Ther. 25, 899–910. https://doi.org/10.1111/cns.13190.
Liu, Q., Li, R., Yang, W., Cui, R., Li, B., 2021. Role of neuroglia in neuropathic pain and depression. Pharmacol. Res. 174, 105957 https://doi.org/10.1016/j.phrs.2021.105957.
Loggia, M.L., Chonde, D.B., Akeju, O., Arabasz, G., Catana, C., Edwards, R.R., Hill, E., Hsu, S., Izquierdo-Garcia, D., Ji, R.R., Riley, M., Wasan, A.D., Zurcher, N.R., Albrecht, D.S., Vangel, M.G., Rosen, B.R., Napadow, V., Hooker, J.M., 2015. Evidence for brain glial activation in chronic pain patients. Brain 138, 604–615. https://doi.org/10.1093/brain/awu377.
Lucas, M., Mirzaei, F., Pan, A., Okereke, O.I., Willett, W.C., O'Reilly, E.J., Koenen, K., Ascherio, A., 2011. Coffee, caffeine, and risk of depression among women. Arch. Intern. Med. 171, 1571–1578. https://doi.org/10.1001/archinternmed.2011.393.
Luo, X., Chen, O., Wang, Z., Bang, S., Ji, J., Lee, S.H., Huh, Y., Furutani, K., He, Q., Tao, X., Ko, M.C., Bortsov, A., Donnelly, C.R., Chen, Y., Nackley, A., Berta, T., Ji, R. R., 2021. IL-23/IL-17A/TRPV1 axis produces mechanical pain via macrophage-sensory neuron crosstalk in female mice. Neuron 109, 2691–2706.e2695. https://doi.org/10.1016/j.neuron.2021.06.015.
Ma, L., Yue, L., Zhang, Y., Wang, Y., Han, B., Cui, S., Liu, F.Y., Wan, Y., Yi, M., 2019. Spontaneous Pain Disrupts Ventral Hippocampal CA1-Infralimbic Cortex Connectivity and Modulates Pain Progression in Rats with Peripheral Inflammation. Cell Rep. 29, 1579–1593.e1576. https://doi.org/10.1016/j.celrep.2019.10.002.
Machado, N.J., Simoes, A.P., Silva, H.B., Ardais, A.P., Kaster, M.P., Garcao, P., Rodrigues, D.I., Pochmann, D., Santos, A.I., Araujo, I.M., Porciuncula, L.O., Tome, A. R., Kofalvi, A., Vaugeois, J.M., Agostinho, P., El, Y.M., Cunha, R.A., Gomes, C.A., 2017. Caffeine Reverts Memory But Not Mood Impairment in a Depression-Prone Mouse Strain with Up-Regulated Adenosine A(2A) Receptor in Hippocampal Glutamate Synapses. Mol. Neurobiol. 54, 1552–1563. https://doi.org/10.1007/s12035-016-9774-9.

Manzhulo, I., Manzhulo, O., Tyrtyshnaia, A., Ponomarenko, A., Konovalova, S., Ermolenko, E., Milkina, E., Starinets, A., 2021. Modulation of Hippocampal Astroglial Activity by Synaptamide in Rats with Neuropathic Pain. Brain Sci. 11 https://doi.org/10.3390/brainsci11121561.

Mapplebeck, J.C., Beggs, S., Salter, M.W., 2017. Molecules in pain and sex: a developing story. Mol. Brain 10, 9. https://doi.org/10.1186/s13041-017-0289-8.

Mills, S.E.E., Nicolson, K.P., Smith, B.H., 2019. Chronic pain: a review of its epidemiology and associated factors in population-based studies. Br. J. Anaesth. 123, e273–e283. https://doi.org/10.1016/j.bja.2019.03.023.

Moesta, A.K., Li, X.Y., Smyth, M.J., 2020. Targeting CD39 in cancer. Nat. Rev. Immunol. 20, 739–755. https://doi.org/10.1038/s41577-020-0376-4.

Moreira-de-Sa, A., Lourenco, V.S., Canas, P.M., Cunha, R.A., 2021. Adenosine A(2A) Receptors as Biomarkers of Brain Diseases. Front. Neurosci. 15, 702581 https://doi.org/10.3389/fnins.2021.702581.

Najjar, S., Pearlman, D.M., Alper, K., Najjar, A., Devinsky, O., 2013. Neuroinflammation and psychiatric illness. J. Neuroinflammation 10, 43. https://doi.org/10.1186/1742-2094-10-43.

Parkhurst, C.N., Yang, G., Ninan, I., Savas, J.N., Yates, J.R.R., Lafaille, J.J., Hempstead, B.L., Littman, D.R., Gan, W.B., 2013. Microglia promote learning-dependent synapse formation through brain-derived neurotrophic factor. Cell 155, 1596–1609. https://doi.org/10.1016/j.cell.2013.11.030.

Pearson-Leary, J., Eacret, D., Chen, R., Takano, H., Nicholas, B., Bhatnagar, S., 2017. Inflammation and vascular remodeling in the ventral hippocampus contributes to vulnerability to stress. Transl. Psychiatry 7, e1160.

Peng, W., Wu, Z., Song, K., Zhang, S., Li, Y., Xu, M., 2020. Regulation of sleep homeostasis mediator adenosine by basal forebrain glutamatergic neurons. Science 369. https://doi.org/10.1126/science.abb0556.

Perry, C.J., Blake, P., Buettner, C., Papavassiliou, E., Schain, A.J., Bhasin, M.K., Burstein, R., 2016. Upregulation of inflammatory gene transcripts in periosteum of chronic migraineurs: Implications for extracranial origin of headache. Ann. Neurol. 79, 1000–1013. https://doi.org/10.1002/ana.24665.

Phelps, E.A., LeDoux, J.E., 2005. Contributions of the amygdala to emotion processing: from animal models to human behavior. Neuron 48, 175–187. https://doi.org/10.1016/j.neuron.2005.09.025.

Rebola, N., Simoes, A.P., Canas, P.M., Tome, A.R., Andrade, G.M., Barry, C.E., Agostinho, P.M., Lynch, M.A., Cunha, R.A., 2011. Adenosine A2A receptors control neuroinflammation and consequent hippocampal neuronal dysfunction. J. Neurochem. 117, 100–111. https://doi.org/10.1111/j.1471-4159.2011.07178.x.

Shackman, A.J., Fox, A.S., Oler, J.A., Shelton, S.E., Davidson, R.J., Kalin, N.H., 2013. Neural mechanisms underlying heterogeneity in the presentation of anxious temperament. PNAS 110, 6145–6150. https://doi.org/10.1073/pnas.1214364110.

Sheng, H.Y., Lv, S.S., Cai, Y.Q., Shi, W., Lin, W., Liu, T.T., Lv, N., Cao, H., Zhang, L., Zhang, Y.Q., 2020. Activation of ventrolateral orbital cortex improves mouse neuropathic pain-induced anxiodepression. JCI Insight 5. https://doi.org/10.1172/jci.insight.133625.

Shichita, T., Hasegawa, E., Kimura, A., Morita, R., Sakaguchi, R., Takada, I., Sekiya, T., Ooboshi, H., Kitazono, T., Yanagawa, T., Ishii, T., Takahashi, H., Mori, S., Nishibori, M., Kuroda, K., Akira, S., Miyake, K., Yoshimura, A., 2012. Peroxiredoxin family proteins are key initiators of post-ischemic inflammation in the brain. Nat. Med. 18, 911–917. https://doi.org/10.1038/nm.2749.

Skaper, S.D., Facci, L., Giusti, P., 2014. Neuroinflammation, microglia and mast cells in the pathophysiology of neurocognitive disorders: a review. CNS Neurol. Disord. Drug Targets 13, 1654–1666. https://doi.org/10.2174/1871527313666141130224206.

Sorge, R.E., LaCroix-Fralish, M.L., Tuttle, A.H., Sotocinal, S.G., Austin, J.S., Ritchie, J., Chanda, M.L., Graham, A.C., Topham, L., Beggs, S., Salter, M.W., Mogil, J.S., 2011. Spinal cord Toll-like receptor 4 mediates inflammatory and neuropathic hypersensitivity in male but not female mice. J. Neurosci. 31, 15450–15454. https://doi.org/10.1523/JNEUROSCI.3859-11.2011.

Sorge, R.E., Mapplebeck, J.C., Rosen, S., Beggs, S., Taves, S., Alexander, J.K., Martin, L. J., Austin, J.S., Sotocinal, S.G., Chen, D., Yang, M., Shi, X.Q., Huang, H., Pillon, N.J., Bilan, P.J., Tu, Y., Klip, A., Ji, R.R., Zhang, J., Salter, M.W., Mogil, J.S., 2015. Different immune cells mediate mechanical pain hypersensitivity in male and female mice. Nat. Neurosci. 18, 1081–1083. https://doi.org/10.1038/nn.4053.

Strange, B.A., Witter, M.P., Lein, E.S., Moser, E.I., 2014. Functional organization of the hippocampal longitudinal axis. Nat. Rev. Neurosci. 15, 655–669. https://doi.org/10.1038/nrn3785.

Sutulovic, N., Veskovic, M., Puskas, N., Zubelic, A., Jerotic, D., Suvakov, S., Despotovic, S., Grubac, Z., Mladenovic, D., Macut, D., Rasic-Markovic, A., Simic, T., Stanojlovic, O., Hrncic, D., 2023. Chronic Prostatitis/Chronic Pelvic Pain Syndrome Induces Depression-Like Behavior and Learning-Memory Impairment: A Possible Link with Decreased Hippocampal Neurogenesis and Astrocyte Activation. Oxid. Med. Cell. Longev. 2023, 3199988. https://doi.org/10.1155/2023/3199988.

Tang, Y.L., Liu, A.L., Lv, S.S., Zhou, Z.R., Cao, H., Weng, S.J., Zhang, Y.Q., 2022. Green light analgesia in mice is mediated by visual activation of enkephalinergic neurons in the ventrolateral geniculate nucleus. Sci. Transl. Med. 14, eabq6474. https://doi.org/10.1126/scitranslmed.abq6474.

Taves, S., Berta, T., Liu, D.L., Gan, S., Chen, G., Kim, Y.H., Van de Ven, T., Laufer, S., Ji, R.R., 2016. Spinal inhibition of p38 MAP kinase reduces inflammatory and neuropathic pain in male but not female mice: Sex-dependent microglial signaling in the spinal cord. Brain Behav. Immun. 55, 70–81. https://doi.org/10.1016/j.bbi.2015.10.006.

Torres, A., Wang, F., Xu, Q., Fujita, T., Dobrowolski, R., Willecke, K., Takano, T., Nedergaard, M., 2012. Extracellular Ca(2)(+) acts as a mediator of communication from neurons to glia. Sci. Signal. 5, ra8. https://doi.org/10.1126/scisignal.2002160.

Tu, Y., Muley, M.M., Beggs, S., Salter, M.W., 2022. Microglia-independent peripheral neuropathic pain in male and female mice. Pain 163, e1129–e1144. https://doi.org/10.1097/j.pain.0000000000002643.

Wang, Q., Kong, Y., Wu, D.Y., Liu, J.H., Jie, W., You, Q.L., Huang, L., Hu, J., Chu, H.D., Gao, F., Hu, N.Y., Luo, Z.C., Li, X.W., Li, S.J., Wu, Z.F., Li, Y.L., Yang, J.M., Gao, T. M., 2021. Impaired calcium signaling in astrocytes modulates autism spectrum disorder-like behaviors in mice. Nat. Commun. 12, 3321. https://doi.org/10.1038/s41467-021-23843-0.

Wang, Y., Liu, N., Ma, L., Yue, L., Cui, S., Liu, F.Y., Yi, M., Wan, Y., 2023. Ventral hippocampal CA1 pyramidal neurons encode nociceptive information. Neurosci. Bull. https://doi.org/10.1007/s12264-023-01086-x.

Wu, Z., He, K., Chen, Y., Li, H., Pan, S., Li, B., Liu, T., Xi, F., Deng, F., Wang, H., Du, J., Jing, M., Li, Y., 2022. A sensitive GRAB sensor for detecting extracellular ATP in vitro and in vivo. Neuron 110, 770–782.e775. https://doi.org/10.1016/j.neuron.2021.11.027.

Yang, Y., Li, H., Li, T.T., Luo, H., Gu, X.Y., Lu, N., Ji, R.R., Zhang, Y.Q., 2015. Delayed activation of spinal microglia contributes to the maintenance of bone cancer pain in female Wistar rats via P2X7 receptor and IL-18. J. Neurosci. 35, 7950–7963. https://doi.org/10.1523/JNEUROSCI.5250-14.2015.

Yue, N., Huang, H., Zhu, X., Han, Q., Wang, Y., Li, B., Liu, Q., Wu, G., Zhang, Y., Yu, J., 2017. Activation of P2X7 receptor and NLRP3 inflammasome assembly in hippocampal glial cells mediates chronic stress-induced depressive-like behaviors. J. Neuroinflammation 14, 102. https://doi.org/10.1186/s12974-017-0865-y.

Zhao, Y., Lin, Z., Chen, L., Ouyang, L., Gu, L., Chen, F., Zhang, Q., 2018. Hippocampal astrocyte atrophy in a mouse depression model induced by corticosterone is reversed by fluoxetine instead of benzodiazepine diazepam. Prog. Neuropsychopharmacol. Biol. Psychiatry 83, 99–109. https://doi.org/10.1016/j.pnpbp.2018.01.011.

Zhao, Y.F., Verkhratsky, A., Tang, Y., Illes, P., 2022. Astrocytes and major depression: the purinergic avenue. Neuropharmacology 220, 109252. https://doi.org/10.1016/j.neuropharm.2022.109252.

Zou, Y., Yang, R., Li, L., Xu, X., Liang, S., 2023. Purinergic signaling: a potential therapeutic target for depression and chronic pain. Purinergic Signal 19, 163–172. https://doi.org/10.1007/s11302-021-09801-x.